EARLY SEAFLOOR SPREADING AND VARIATIONS IN

CRUSTAL ACCRETION IN THE LAU BASIN

A THESIS SUBMITTED TO THE GRADUATE DIVISION OF THE UNIVERSITY
OF HAWAI'I AT MĀNOA IN PARTIAL FULFILLMENT OF THE REQUIREMENTS
FOR THE DEGREE OF

MASTER OF SCIENCE

IN

GEOLOGY AND GEOPHYSICS

DECEMBER 2012

By

Regan Austin

Thesis Committee:

Fernando Martinez, Chairperson
Richard Hey
Paul Wessel

Acknowledgements

Abstract

Recent geophysical mapping of the western Lau Basin in combination with previously interpreted data has provided a more detailed picture of the basin's early opening history. This thesis focuses on updated compilations of bathymetric, magnetic field and acoustic imagery data in combination with petrologic and seismic data. Expanding on previous magnetic inversions [*Taylor et al.*, 1996; *Zellmer and Taylor*, 2001] which account for the influence of field skewness and bathymetric relief on the magnetic field, inversion of additional data has led to a new seafloor magnetization map of the basin. This, in conjunction with bathymetric data, resolves distinct terrains throughout the basin, including abyssal hill fabric in the western basin. These N-S oriented ridges and their affiliated magnetic anomalies indicate that organized seafloor spreading initiated earlier in the basin's history than previously interpreted, along now extinct spreading centers in the western basin. Other variations in the fabric of the western basin can be attributed to a broad array of processes beyond rifting and organized spreading, including hummocky terrain indicative of diffuse magmatism and seamounts that may once have been a proto-arc for the nascent basin. A variety of morphologies is not only found within the western basin, but throughout the Lau Basin. This range is evidence that the opening history involved a diversity of crustal production mechanisms due to abrupt variations in the underlying mantle wedge from which crust formed.

Table of Contents

Table List

Figure List

1. Introduction

A backarc basin forms adjacent to a subduction zone when extension occurs in an otherwise convergent setting, either through rollback of the down-going plate or retreat of the overriding plate away from the trench [*Carlson and Melia*, 1984; *Moberly*, 1972]. This extension causes rifting and the formation of new oceanic crust from magmatic crustal accretion within the overriding plate. A new plate forms between the locus of extension and the trench. Rifting can occur behind the arc, within the arc, or in the forearc, often resulting in the formation of two ridges from a once contiguous volcanic arc.

While backarc spreading centers are typically similar to mid-ocean ridges, the extent of melting and the rheology of the underlying mantle can greatly influence the manner of crustal accretion. Water content and concentration of materials transported by the subducting slab decrease with distance from the trench, in the direction of the backarc basin, leading to heterogeneity within the mantle wedge. As backarc spreading centers can be found at a range of distances from the arc, their lavas are influenced by compositional changes in the underlying melt source. The morphologic, geologic, geophysical, and geochemical characteristics of backarc spreading centers reflect the nature of the underlying mantle wedge at the time they formed. We can use such observations to learn about both the nature of the mantle wedge and the effects of varying mantle chemistry on seafloor spreading characteristics.
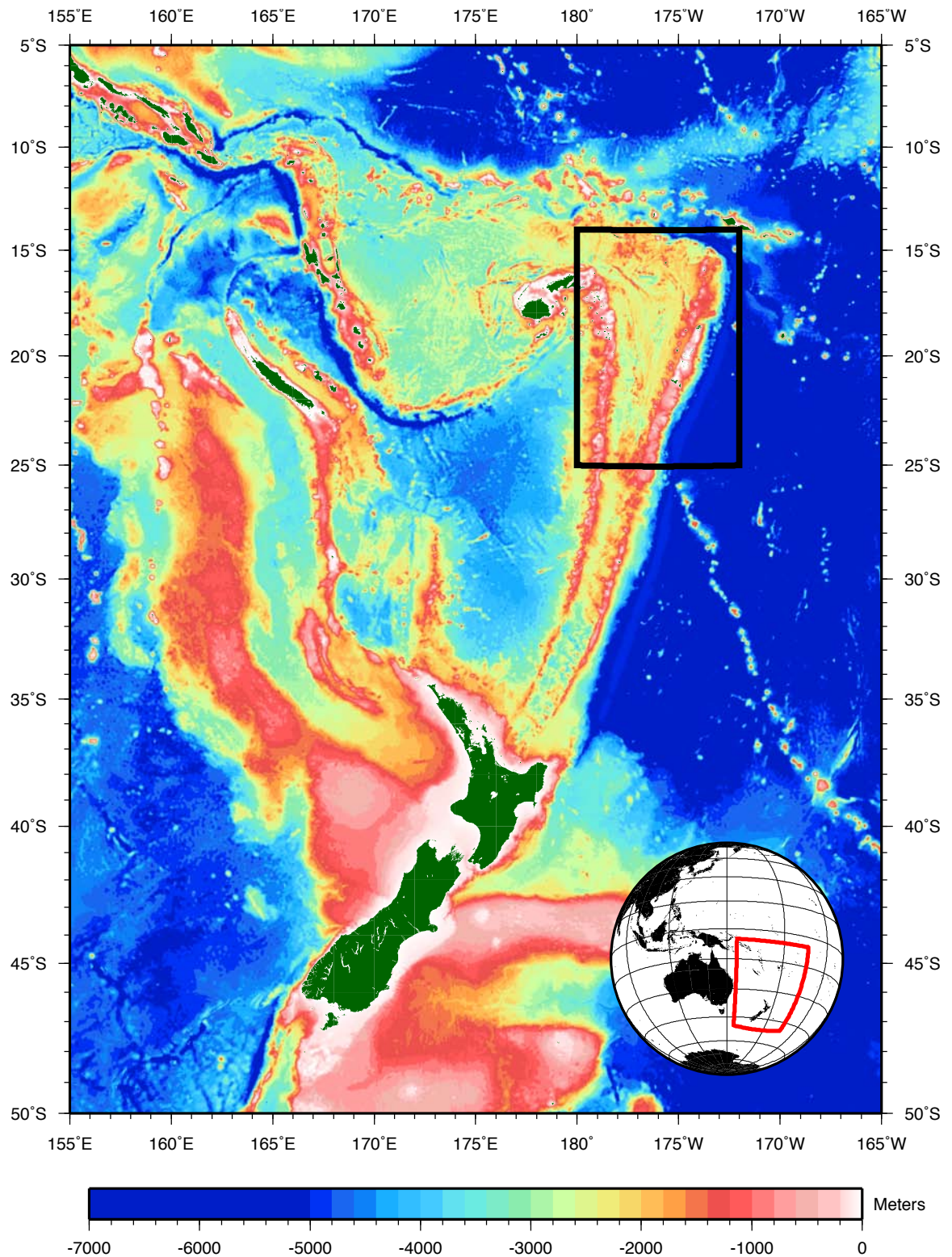
Figure 1.1. Regional Bathymetric map of the Lau Basin-Havre Trough-Taupo Rift complex. Data are taken from the 1-arc-minute predicted bathymetry grid of

Smith and Sandwell [1997]. The inset map shows the location on the globe. Subaerial features such as islands are in dark green.

1.1 This Study

In this thesis I examine the characteristics of crustal accretion across the Lau Basin, from its early development in the western basin to the better described active spreading centers in the central and eastern basin. Recent geophysical data collected in the western basin show that crustal morphology is highly variable, and includes abyssal hill fabric, hummocky terrain, seamounts, and a shallow platform. Within the central and eastern basin, the updated bathymetric data compilation displays morphologic variations not only along axis, but also with distance from the axes, between shallower, inflated terrain and deeper, flatter terrain. A new whole-basin magnetic inversion displays patterns ranging from linear to discontinuous often correlating to the identified terrains. These geophysical variations are generally consistent with chemical variations in sampled lavas as well.

Evidence indicates that organized spreading initiated adjacent to the Lau Ridge, early in Lau Basin history. Distinct morphologic provinces illuminate different geologic processes active during early basin opening. Not only do these provinces reflect different tectonic events that have occurred, they also reflect volcanic variations indicative of changes in their mantle wedge source. Despite irregularity, short sections of lineated magnetic anomalies and abyssal hill fabric support an organized seafloor spreading interpretation for parts of the western basin. Other terrains in the western basin lack lineated magnetic anomalies but have distinctive volcanic morphologies, contrasting with a purely rifting origin for the early basin. We therefore interpret a largely magmatic early

3

basin opening history after a brief phase of rifting to break up the Lau-Tonga arc complex.
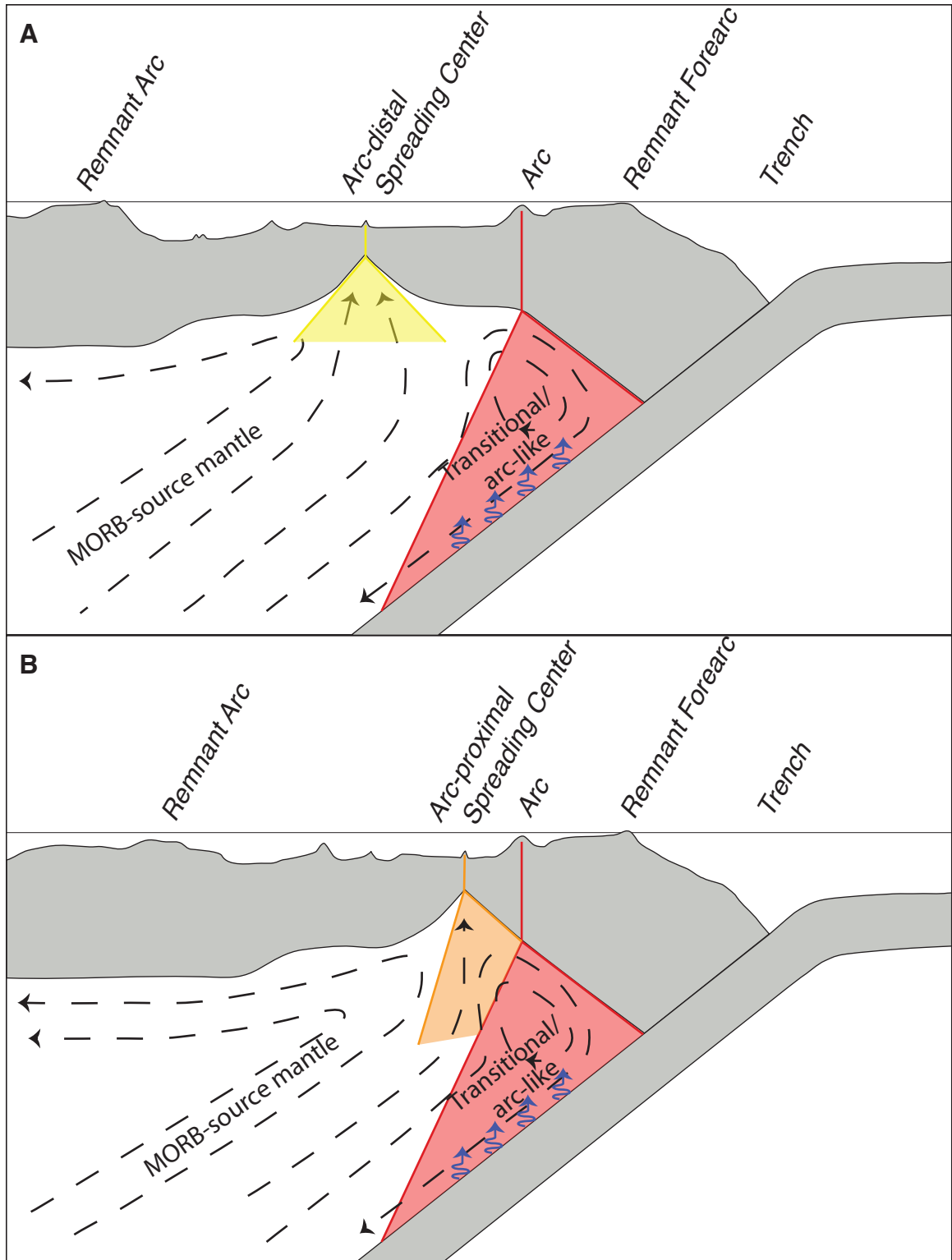
Figure 1.2. Schematic bathymetric cross sections of a subduction zone and backarc basin across **(A)** an arc-distal spreading center (>100 km) and **(B)** an arc-proximal spreading center (<50 km). Dashed arrows demonstrate flow within the mantle and blue wavy arrows indicate material (including water and other volatiles) entering the mantle from the subducting slab. Red signifies the arc's melt regime, yellow signifies the melting regime below a spreading center with no arc influence, and orange signifies the arc-influenced spreading center melt regime. As proximity of the axis to arc volcanoes increases, slab material is incorporated into crustal formation along spreading centers.

As formation of the central and eastern parts of the basin is primarily attributed to organized crustal accretion, most variations within these domains reflect changes in melt supply related to mantle wedge composition. Small-scale variations within different domains of the basin indicate that these changes in the mantle wedge are abrupt. In addition to the broad distribution of currently active spreading centers, crustal accretion and tectonic reorganization have altered the arc proximity of spreading centers throughout the opening history of the basin. Thus, crustal formation in the Lau Basin has sampled the mantle wedge in numerous locations, demonstrating its heterogeneity.

1.2 Background

The original Lau-Tonga arc complex formed behind the Tonga Trench due to westward subduction of the Pacific Plate beneath the overriding Australian Plate. Forearc rifting of the Lau-Tonga arc complex initiated about 6 Ma [*Hawkins et al.*, 1994] when rollback of the subduction hinge away from the Australian Plate allowed for extension [*Hawkins and Melchior*, 1985]. This corresponds to the cessation of southward subduction of the Pacific Plate along the northern margin of the Australian Plate, and the subsequent change in Pacific plate motion at 6 Ma, which is generally attributed to failed

subduction of the Ontong Java Plateau [*Austermann et al.*, 2011; *Wessel and Kroenke*, 2000; 2007]. Rifting of the arc complex resulted in the formation of the Lau Basin between the now separate Tonga and Lau Ridges, and the new Tonga Plate. As the Tonga Ridge has moved eastward relative to the Lau Ridge, the Lau Ridge has apparently remained passively attached to the Australian Plate. Currently, neither ridge is magmatically active; arc volcanism now occurs along the eastern edge of the basin, at the Tofua Arc. Extensional volcanism takes place along spreading centers throughout the basin. While Australia-Pacific convergence is approximately 80 mm/yr, convergence rates between the Tonga and Pacific Plates are the fastest rates observed in the world, increasing northward from 150 to 250 mm/yr (possibly due to rapid rollback), and extension between the Australia and Tonga Plates increases from 80 to 165 mm/yr as determined by GPS [*Bevis et al.*, 1995; *Phillips*, 2003]. Faster extension to the north led to the basin opening in a wedge-like fashion. Ruellan et al. propose that the southward decrease in spreading rates is due to "locking" of southern basin opening by subduction of the Louisville Seamount Chain [2003], which intersects the trench near 26°S.

The mechanisms of backarc extension within the basin have been debated extensively and various models have been proposed. Karig first proposed that backarc basins formed through extensional processes occurring adjacent to subduction zones [1970]. He suggested that the Lau and Tonga ridges had once been a contiguous feature, before the Lau Basin formed between them via mechanisms similar to those that typically form oceanic crust. Subsequent studies discovered evidence of recent magmatic accretion through young, basaltic dredged rocks, magnetic anomalies, and plate boundaries similar to those found in mid-ocean ridge (MOR) settings [*Gill*, 1976; *Lawver et al.*, 1976;

Weissel, 1977]. However, based on estimates of sediment thickness, Katz suggested a process of "oceanization" that didn't require substantial extension [1978]. Instead, he proposed that existing shallow crust had collapsed to form the basin and successive magmatic intrusion led to its oceanic appearance. The analogy to mid-ocean ridge-like processes was also challenged by evidence of diffuse tectonics, including the irregular character of magnetic anomalies [*Lawver and Hawkins*, 1978] and shear dominated seismicity within the basin [*Hamburger and Isacks*, 1988].

Early sidescan sonar mapping (GLORIA) in addition to petrologic data from Ocean Drilling Program (ODP) Leg 135 cores and dredging surveys enabled new insights into the basin. Two distinct tectonic domains (the western and central basins), and a clear locus of spreading were identified [*Hawkins*, 1995; *Hawkins and Melchior*, 1985; *Hawkins and Allan*, 1994; *Parson et al.*, 1992; *Parson et al.*, 1990]. While western basin formation was attributed to a protracted rifting phase, a 2-stage ridge-propagation model was suggested for eastern basin formation, in which the East Lau Spreading Center (ELSC) propagated southward and was succeeded by propagation of the Central Lau Spreading Center (CLSC). Evidence of rifting from seismic reflection data (including possible block-faulting) was limited to the western basin, leading to a more complex 5-stage model involving coeval phases of rifting and spreading throughout the Lau-Havre-Taupo complex [*Parson and Wright*, 1996; *Parson et al.*, 1994]. Plate motions were constrained with geodetic data [*Bevis*, 1997; *Bevis et al.*, 1995; *Phillips*, 2003], and an inversion of bathymetry and magnetic data clearly resolved magnetic isochrons within the basin for the first time, demonstrating its similarity to mid-ocean ridges [*Taylor et al.*, 1996]. Opening rates along active spreading centers determined from magnetic anomalies

appeared much lower than velocities determined by geodetic data; however, seismic data [*Pelletier et al.*, 1998] and the recognition of a Fonualei spreading center in the northern basin led to the proposal of the Niuafo'ou Microplate as part of a 3-plate kinematic model [*Zellmer and Taylor*, 2001]. This new model resolved previous discrepancies [*Bevis et al.*, 1995; *Taylor et al.*, 1996] between geodetically- and magnetically-determined spreading rates in the Lau Basin.

Recent work in the Lau Basin and Havre Tough to the south has shown that backarc basin crustal production can be highly variable [*Fujiwara et al.*, 2001; *Watanabe et al.*, 2010; *Wysoczanski et al.*, 2010]. Organized spreading within the basin is complicated by variability of along-axis terrain formed at currently active spreading centers. At mid-ocean ridges, morphologic variations (caused by variations in magma supply) are typically correlated to spreading rates. In the Lau Basin, these variations are instead correlated to arc-proximity, though the changes in melt production that cause these variations are alternately attributed to decompression melting [*Conder et al.*, 2002; *Harmon and Blackman*, 2010] or increased water content [*Dunn and Martinez*, 2011; *Martinez and Taylor*, 2002; 2003; 2006] within the mantle wedge. Furthermore, many studies highlight an off-axis "ridges and knolls" terrain with proposed interpretations ranging from formation through magmatic injection into rifted crust to some form of diffuse crustal accretion [*Fujiwara et al.*, 2001; *Martinez et al.*, 2006; *Watanabe et al.*, 2010; *Wysoczanski et al.*, 2010]. It is apparent that magmatism within the basin is not isolated to organized spreading centers. These observations led to new models for crustal accretion in backarc basins that could explain the variable topography throughout the basin as a result of variations in magmatism and its mode of emplacement.
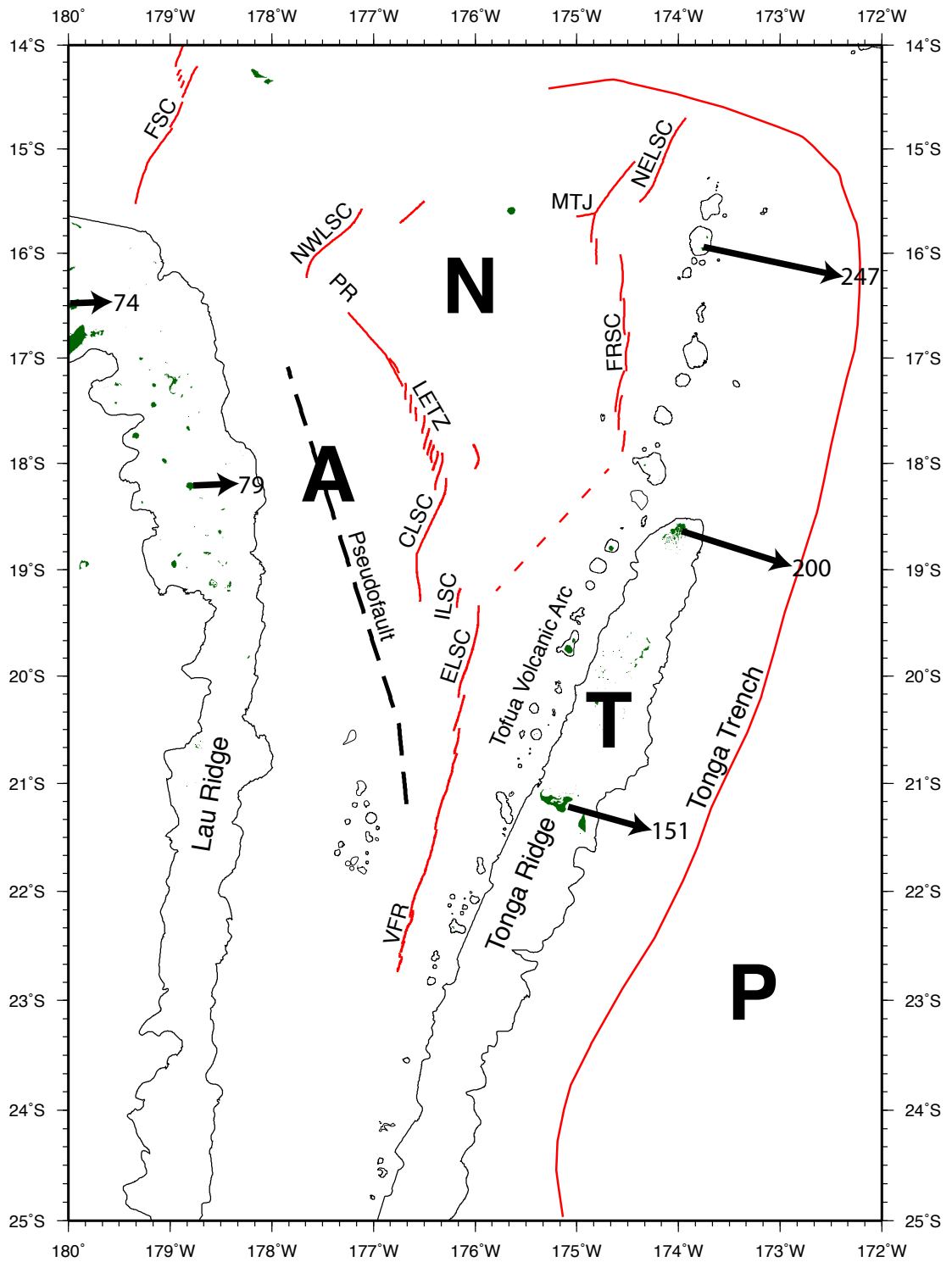
Figure 1.3. Tectonic map of the Lau Basin. Red lines indicate plate boundaries, the black dashed line indicates the pseudofault separating the western and central basins, and subaerial features are in dark green. Tofua Arc volcanoes are

outlined with 800-m contours, while the Lau Ridge, the Tonga Ridge, and western basin seamounts are outlined with simplified 1,450-m contours. GPS-derived plate motions in a Pacific-fixed reference frame are identified by black arrows labeled with velocities in mm/yr [*Phillips*, 2003]. Abbreviations of plates are as follows in large, bold letters: A = Australia, N = Niuafoʻou, T = Tonga, P = Pacific. Abbreviations of tectonic features are as follows: CLSC = Central Lau Spreading Center, ELSC = Eastern Lau Spreading Center, FRSC = Fonualei Rift and Spreading Center, FSC = Futuna Spreading Center, ILSC = Intermediate Lau Spreading Center, LETZ = Lau Extensional Transform Zone, MTJ = Mangatolu Triple Junction, PR = Peggy Ridge, NELSC = Northeast Lau Spreading Center, NWLSC = Northwest Lau Spreading Center, VFR = Valu Fa Ridge.

Over time the Lau Basin underwent abrupt changes in the locus of extension. Initial extension began about 6 Ma in the western basin adjacent to the Lau Ridge [*Hawkins and Allan*, 1994]. Development of the western basin was truncated by the southward propagating ELSC from ~4 Ma onward [*Taylor et al.*, 1996]. Propagation formed the pseudofault bounding the western basin while seafloor spreading progressed and arc magmatism migrated eastward. Starting ~2 Ma, the Lau Extensional Transform Zone (LETZ) and CLSC replaced the former northern ELSC in a second major southward propagation event [*Parson and Hawkins*, 1994; *Taylor et al.*, 1996]. Today, it appears the Valu Fa Ridge (VFR) continues propagating southward, though it is propagating into magmatically active, if not organized, terrain.

The early history of the basin, represented by the western basin (adjacent to the Lau Ridge), has been especially difficult to resolve. While a "Western Lau Spreading Center" was once suggested [*Parson et al.*, 1990], the western Lau Basin crust has generally been attributed to a phase of broad and protracted arc rifting. This contrasts with the interpretation of many other backarc basins; however, irregular terrain and lack of identifiable magnetic lineations led to this explanation.

2. Methods

Shipboard collection of bathymetry, magnetic field and sidescan sonar data was undertaken in the western Lau Basin in 2009. These data were combined with earlier transit and archive data to supplement coverage. Surveys were processed individually and combined with data sets previously collected throughout the region.

Table 2.1. Shipboard data compilation. Data from the following cruises were added to the magnetic anomaly data compilation of Zellmer and Taylor [2001].

Ship Name	Cruise No.	Year	Area	Reference
R/V Yokosuka (Japan)	LAUHAVRE 97	1997	S. Lau, Havre Tr.	[*Fujiwara et al.*, 2001]
R/V L'Atalante (Fr.)	ALAUFI 2000	2000	Futuna SC	[*Pelletier et al.*, 2001]
R/V Kilo Moana	KM0410	2004	Western Basin	[*Martinez et al.*, 2006]
R/V S. Surveyor (Aus.)	SS200807	2008	LETZ, NWLSC	[*Arculus*, 2008]
R/V Marcus Langseth	MGL0903	2009	Western Basin	[*Dunn and Martinez*, 2011]
R/V Onnuri (S. Korea)	n/a	2009	Western Basin	n/a
R/V Roger Revelle	RR0915	2009	Western Basin	n/a

2.1 Bathymetry

Multibeam bathymetry data from the surveys were processed using MB System [*Caress and Chayes*, 2006] and GMT software package (version 4.4.0) [*Wessel and Smith*, 1998]. Multiple passes in many locations increased ping density, enabling noise reduction and improved resolution. Individual points (longitude, latitude, depth) were extracted from the multibeam files using MB-System software. Data were spatially merged and then filtered using the following automated procedure to remove noise spikes. The combined data were first filtered using a median filter (GMT program *blockmedian*) and gridded (GMT program *xyz2grd*) in 0.001 degree cells.
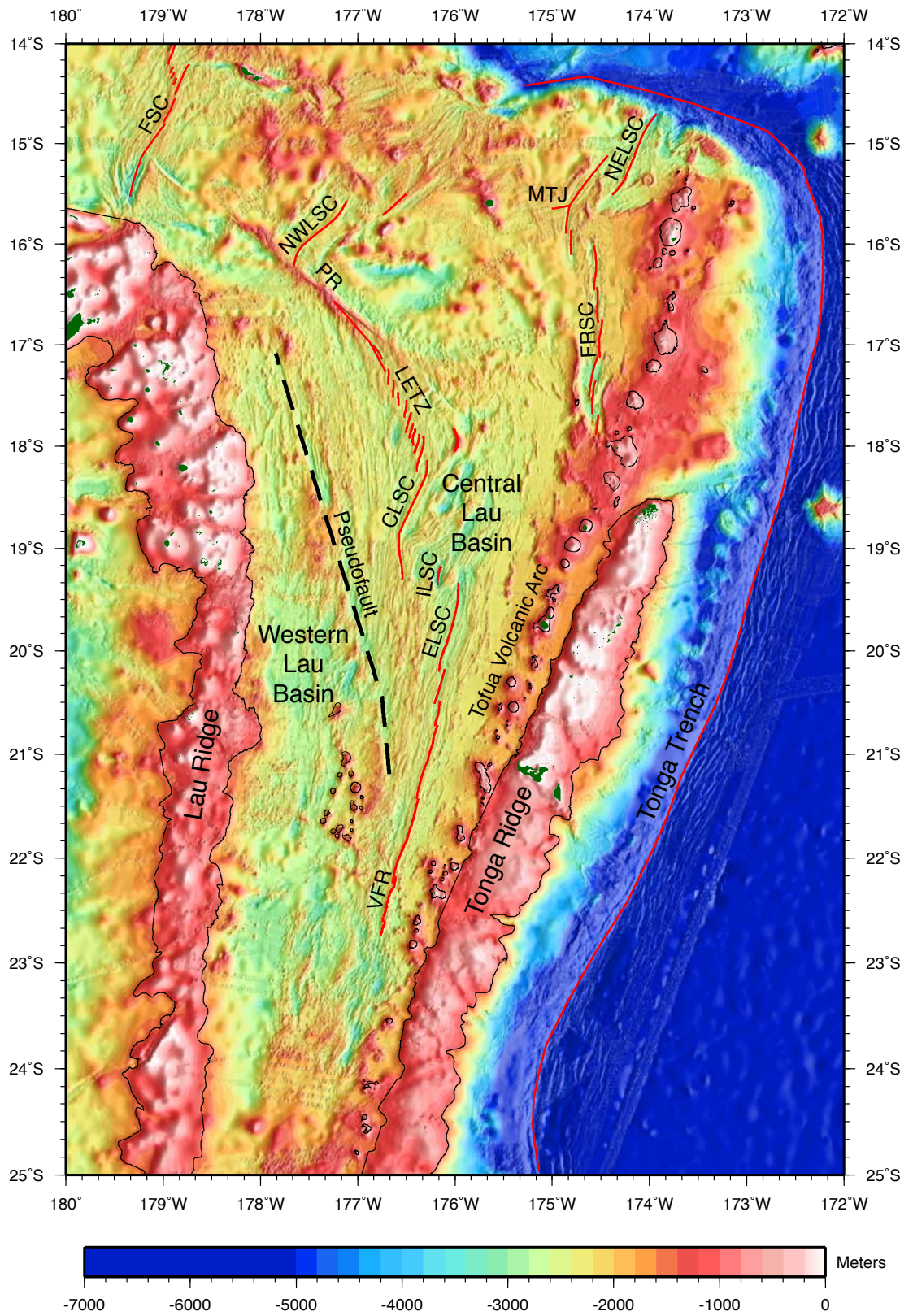
Figure 2.1. Compiled Bathymetry of the Lau Basin with currently recognized plate boundaries and other tectonic features. Shipboard bathymetry is gridded at

12

0.001-degree resolution, combined with 1-arc-minute predicted bathymetry from satellite altimetry data, and illuminated from the east. Symbols and abbreviations are as in Figure 1.3.

The gridded data were then plotted and inspected. Noise (outliers) typically constituted negative spikes consisting of individual points or small numbers of points near swath edges. If these were present the grid was then re-filtered (using GMT program *grdfilter*) with a median filter, increasing the filter width by 3, 5 or 7 cell widths until no noise spikes were evident in the grid. This smooth surface was then used as a reference for passing or rejecting the original individual point data. Each extracted data point was compared to the reference surface and retained if it fell within +100 or -20 m of the reference grid. The procedure used GMT program *grdtrack* to sample the smooth reference grid at the locations of individual point data and the UNIX program *awk* to perform the test. Asymmetric tolerance limits were chosen by inspection after several test runs and because most outliers consisted of deep "pits" rather than shallow "spikes". These tolerance limits also prevented cutting off of real values near the shallow crests of features, which tended to be sharper than their lower boundaries in the filtered reference grid. The multibeam points that passed this test were then gridded in 0.001-degree cells using GMT program *xyz2grd*. These cleaned, gridded data were filtered once more with *grdfilter* and a 5-cell window to fill in small data gaps. The original cleaned grid was superimposed on this filtered grid using *grdmath*. This produced a grid that retained the resolution of the 0.001-degree gridding but had small gaps filled by interpolation.

One-arc-minute predicted bathymetry data from satellite altimetry measurements [*Smith and Sandwell*, 1997] were interpolated and re-gridded at 0.001 degree using GMT program *grdsample*. The multibeam grid was then superimposed on this grid using GMT

13

program *grdmath*, so that predicted bathymetry values would fill in data gaps between multibeam swaths. The resulting grid then had no gaps with full 0.001-degree resolution multibeam data overlaid on interpolated 1-arc-minute predicted bathymetry values.

In preparation for a magnetization inversion, this higher resolution bathymetry grid was reduced to 0.5-arc-minute spacing using a boxcar filter (GMT program *grdfilter*). Land values and depths shallower than 500 m were clipped to 500 m (GMT program *grdclip*) as a requirement of the inversion technique that the magnetic field values lie completely above the source layer.

2.2 Magnetics

Raw magnetic total field data collected in 2009 (*Table 2.1*) were merged with navigation data and median filtered to one-arc-minute intervals in time (using GMT function *filter1d)*. The 2009 International Geomagnetic Reference Field model (IGRF) was subtracted from total field values, yielding the magnetic anomaly. IGRF was used instead of CM4 (a more detailed model accounting for diurnal variations), as CM4 is not available for the period in which shipboard surveys took place. A crossover analysis was performed on the anomaly field values to determine offsets between surveys. Data that were deemed more reliable (KM0410) were used as a standard, and the average discrepancies with this cruise were removed from other data sets as a simple DC shift. This set of cruise data was then combined with previously collected shipboard surveys and the shipboard 3-arc-minute World Digital Magnetic Anomaly Map (WDMAM) for the region, which includes leveled NGDC data, to increase coverage [*Maus et al.*, 2007].
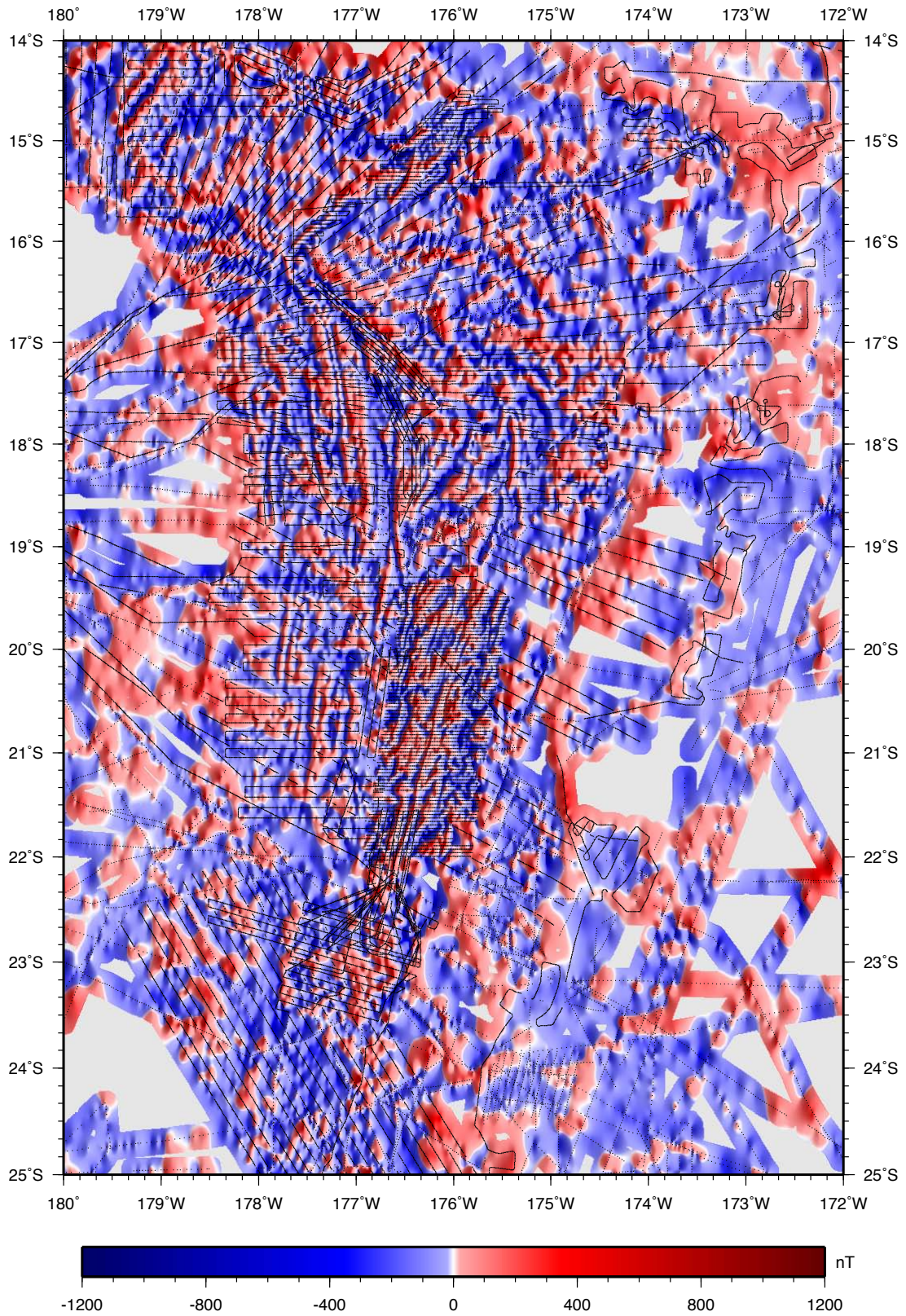
Figure 2.2. Magnetic field anomaly of the Lau Basin compiled from shipboard data, aeromagnetic data and WDMAM data. Data are gridded at 0.5-arc-minute

resolution, but WDMAM data points are spaced at 3 arc minutes. The grid is illuminated from the east and contributing data points are displayed as black dots. Areas without data are light gray.

Aeromagnetic data in the region [*Cherkis*, 1980], collected at an altitude of 330 m, showed significant discrepancies with the ship data, even after cross-over correction, due to apparent navigational errors in the data, which were collected in 1979. The aeromagnetics data were gridded and downward continued (using GMT program *grdfft*) and then resampled at the original data locations, but no significant improvement was found in the discrepancies with ship data. Because of the low altitude of the aeromagnetics data (~330 m) relative to predominant water depths in the areas of interest (2,000-3,000 m) the original data were used in subsequent analysis without downward continuation. An attempt was made to correct navigational errors using a grid search method to determine the spatial shift that most reduced crossover errors with ship data. The adjusted aeromagnetic data still had significant crossover errors with the ship data and were only used in gap areas where no other data were available.

Where WDMAM or aeromagnetics data and individual surveys overlap, individual surveys were given precedence, followed by WDMAM data, and other data were masked out. All total field anomaly data were reduced to 0.5-arc-minute spacing (using GMT program *blockmedian*) and gridded at 0.5-arc-minute spacing using, a minimum curvature routine (GMT program *surface*) [*Wessel and Smith*, 1991]. Areas more than 6 arc minutes from data points in this grid were tapered to zero using a masking grid. The masking grid had values of 1 within 6 arc minutes of data points and 0 elsewhere. It was tapered using a 1.5-arc-minute boxcar filter. The masking grid was multiplied with the data grid to produce the tapered data grid used in the magnetization

inversion. This avoided large amplitude anomalies that can result from minimum

curvature fitting in areas without data control.

2.2.1 Inversion and Magnetization Map

A Fourier inversion of the 0.5-arc-minute magnetic field and bathymetry grids

was performed in order to calculate seafloor magnetization [*Macdonald et al.*, 1980;

Parker and Huestis, 1974] using the Mirone software package [*Luis*, 2007]. This

inversion also accounted for skewness in the magnetic field of the earth based on the

2005 IGRF model, an average to account for the broad range in survey dates. While

variations in crustal thickness are expected [*Dunn and Martinez*, 2011], the effect on the

magnetic source layer is unknown, so a constant magnetic source layer thickness of 0.5

km was assumed. Grids were mirrored within Mirone to reduce edge effects. Results of

the inversion were tapered to zero using the same mask used on the data to remove

interpolated values away from data values. As the inversion procedure assumes that the

magnetization vector is produced by an axial geocentric dipole, there are some limitations

to this method. Crustal blocks that have undergone tectonic rotation following formation

may display magnetization patterns that are inversely or more weakly magnetized

compared to their original magnetization. Furthermore, calculating a magnetization

results in a non-unique solution. This non-uniqueness is expressed as a magnetization

solution for the given topography that produces no field at the level of the measurements.

It is termed an "annihilator" [*Blakely*, 1996; *Parker and Huestis*, 1974] and any quantity

of it may be added to the inversion. The quantity of magnetic annihilator added was

chosen to balance the polarity intensities across the Brunhes Chron following the method

of Macdonald et al. [1980] *(see appendix)*.

17
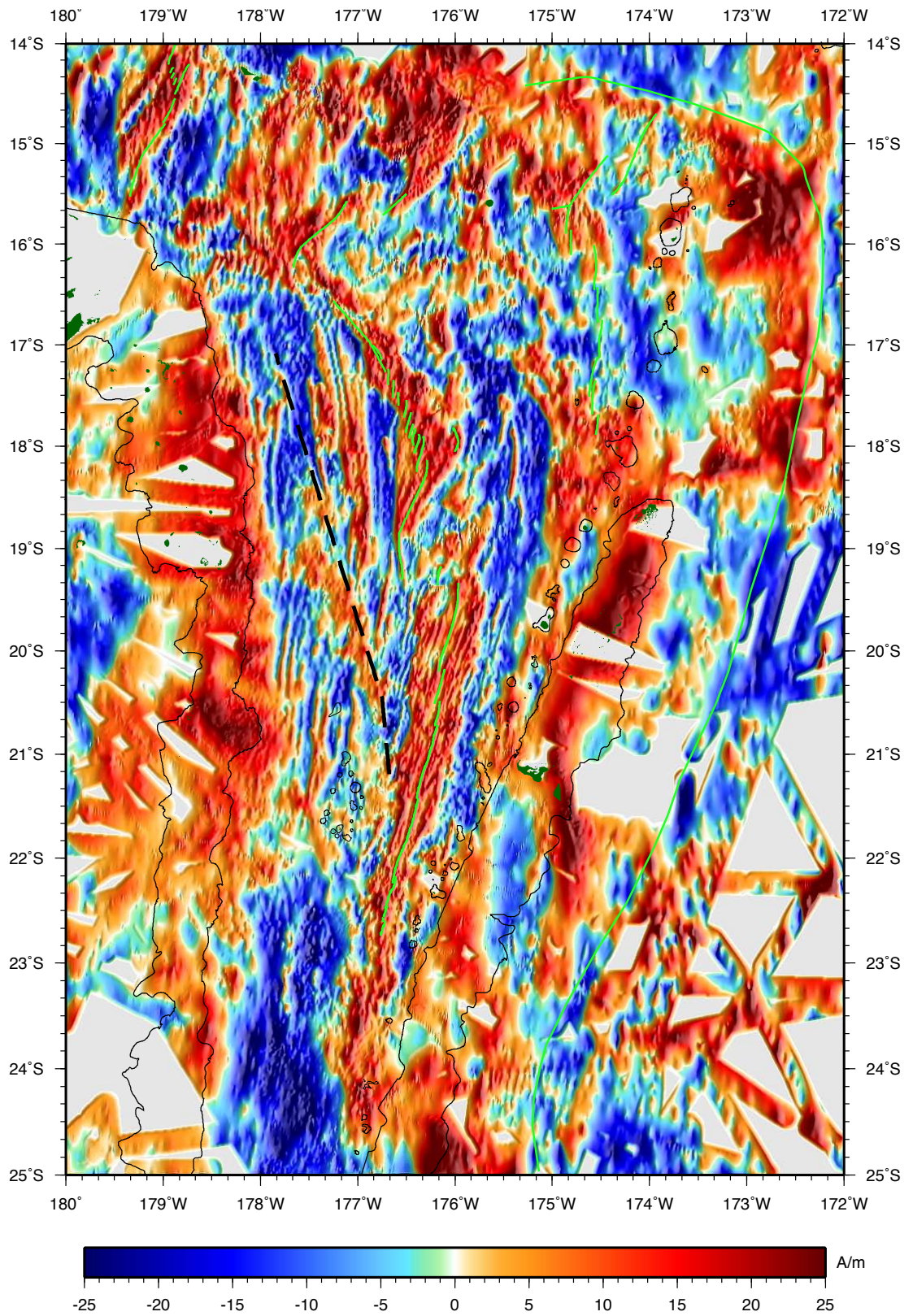
Figure 2.3. Estimated seafloor magnetization of the Lau Basin from inversion of the magnetic field anomaly data with bathymetry. Bathymetry was reduced to

0.5-arc-minute resolution and points shallower than 500 m were clipped to 500 m for the inversion, which assumed a 0.5-km source layer. The grid is illuminated from the east, and areas without data are light gray. Light green lines indicate plate boundaries, and other symbols are as in Figure 1.3.

2.3 Acoustic Imagery

Because the amplitude data provide a qualitative measure of the relative backscatter intensity of the seafloor (depending on system used, insonification direction with respect to local seafloor geometry, power settings, etc.), only a visually guided attempt was made to combine acoustic amplitude data from various cruises to map the study area. Acoustic backscatter intensities were processed from individual cruises using MB-System[*Caress and Chayes*, 2006]. MB-System utilities *mbbackangle* and *mbprocess* were used to reduce the nadir and other artifacts. Individual amplitude data points were extracted using *mblist* and were then median filtered in 0.001-degree cells for each cruise. Data in each grid were scaled to a common range (0-255) using GMT program *grdmath*, compared at overlaps, and then average discrepancies between cruises were removed. The various data sets were then combined and added to the previous compilation of Zellmer and Taylor [2001] to make the map shown in *Figure 2.4*.
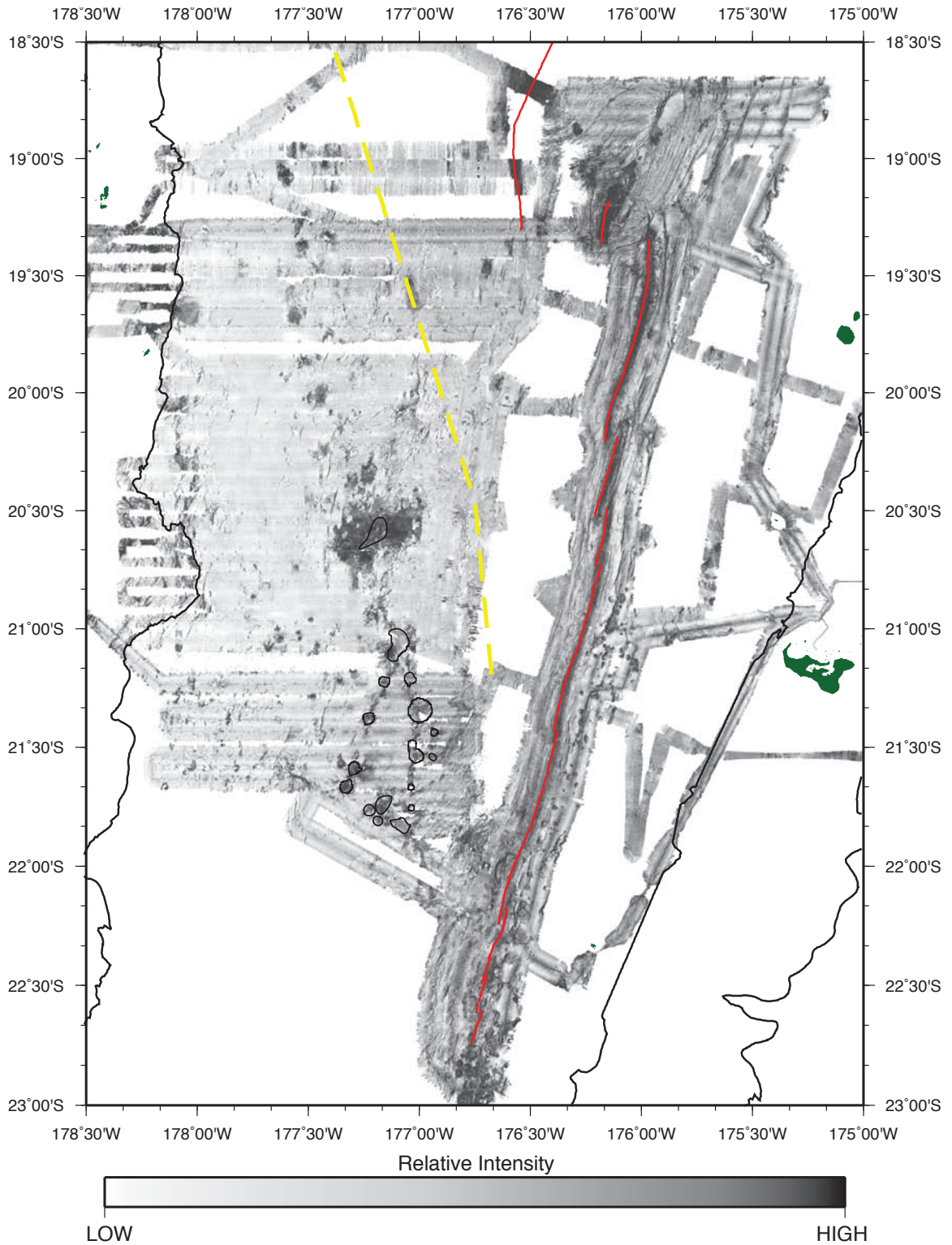
Figure 2.4. Acoustic reflectivity of the western Lau Basin and active spreading centers. High reflectivity is black and low reflectivity is light gray. Data were gridded at 0.001. Red lines indicate plate boundaries, the pseudofault is represented by a dashed yellow line. Other symbols are as in Figure 1.3.

20

3. Results

Our new data expand on previous bathymetry and magnetic compilations for the Lau Basin [*Taylor et al.*, 1996; *Zellmer and Taylor*, 2001]. We focus on the early opening development in the western part of the central basin, which previous studies did not address due to lack of data, and we also touch on new mapping throughout the basin. The Lau Basin consists of various distinct tectonic domains. From west to east, these are the Lau Ridge, the western basin, a pseudofault, the central basin, the Tofua Arc, the Tonga Ridge, and the Tonga Trench (*Figure 3.1*). The northern basin is discussed, but it is not adequately mapped for extensive analysis in this study.
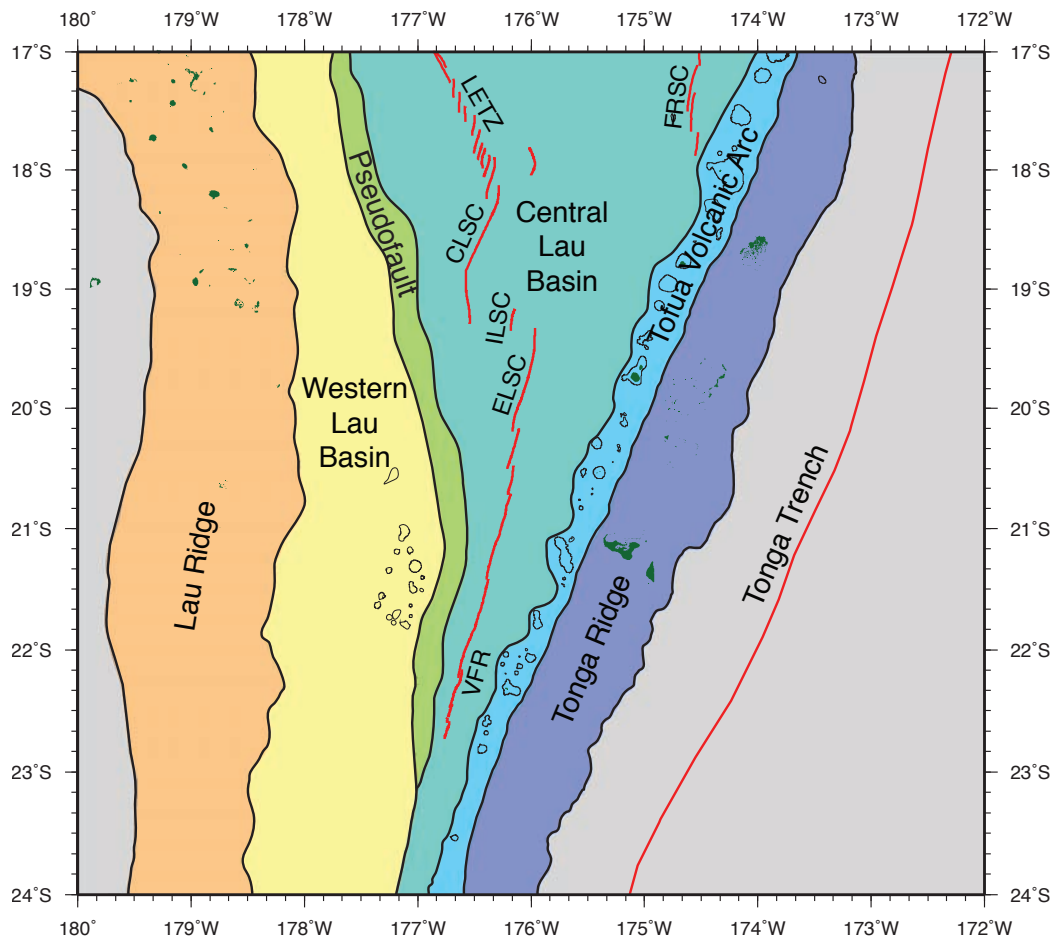
Figure 3.1. Tectonic domains of the Lau Basin. Plate boundaries are in red, and subaerial features in dark green. Tofua Arc volcanoes are outlined with 800-m contours, while western basin seamounts are outlined with 1,450-m contours.

3.1 Lau Ridge

The Lau Ridge remnant arc bounds the Lau Basin to the west. Earliest volcanism has been dated at approximately 30 Ma, but could range from late Eocene to early Oligocene [*Whelan et al.*, 1985]. Volcanism on the Lau Ridge continued into the early stages of basin opening, as late as 3 Ma. While much of the Lau Ridge history is characterized by eruption of andesitic to dacitic lavas [*Gill*, 1976], this late stage of volcanism was increasingly basaltic [*Whelan et al.*, 1985]. Basin surveys generally stop at the eastern margin of the Lau Ridge, leaving only sparse ship transit lines transecting the ridge. Predicted bathymetry from satellite altimetry supplements these. Some recent surveys have continued a short distance onto the ridge, mapping the eastern margin in more detail.
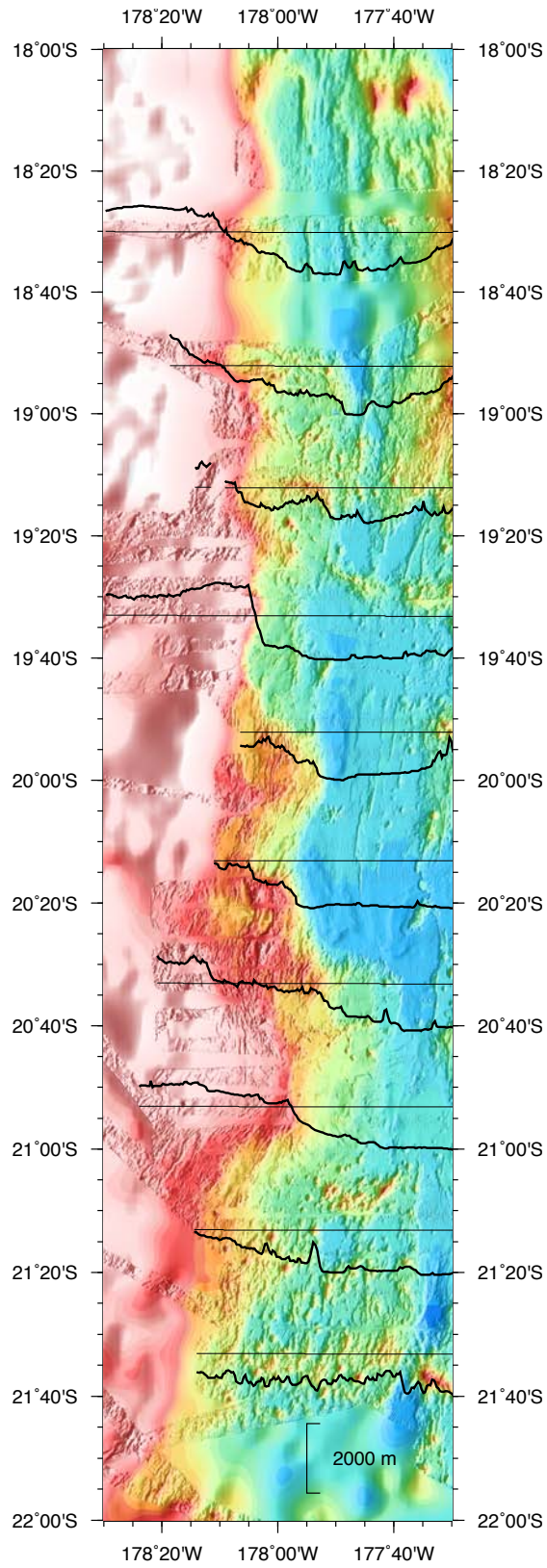
Figure 3.2. Bathymetry of the eastern Lau Ridge margin. Cross sections sampling bathymetry are displayed with thick black lines, while 1,500-m baselines are displayed with fine black lines. Cross sections indicate that the transition from ridge to basin is highly variable.

The Lau Ridge forms an irregular high with depths near 500 m. It is generally oriented N-S; however, north of 19º30'S it gradually curves westward. This northern section is broader (>100 km wide) and has numerous islands, while the southern section forms a narrower (50-75 km wide), more irregular ridge with few islands. To the south, the ridge is largely submarine with few islands and shoals. The eastern bounding slope of the ridge varies between steep and more gradual descents toward the basin floor. Along the steeper slopes, depths rapidly transition from shallower than 1,000 m on the ridge to deeper than 2,000 m within the basin and then remain approximately constant across the basin, excluding seamounts. Along gradual slopes, there is some evidence of landslides, with N-S trending scarps parallel to the ridge. The western bounding slope has very limited mapping, but satellite altimetry indicates it is highly variable, with a sinuous edge and discrete seamounts.

The magnetization inversion along the Lau Ridge generally shows strong, positive values, often exceeding 15 A/m though data are sparse and the ridge is generally too shallow for proper resolution as track line spacing becomes much wider than the water depth. Acoustic imagery data are sparser, but where it is available, they show high reflectivity on the steep slopes and where scarps are apparent.

3.2 Western Basin

The western basin is bounded on the west by the Lau Ridge, and on the east by the pseudofault formed when the ELSC propagated southward. It widens from approximately 50 km in the north to 200 km in the south, in conjunction with the SSE trend of the pseudofault. The floor of the basin is generally 2,500-3,000 m deep but shoals to 1,500 m or shallower along the eastern edge and at various seamounts. Seismic reflection profiles and ODP cores indicate that some volcaniclastic and biogenic sediment infill has occurred throughout the western basin [*Parson et al.*, 1992; *Shipboard Scientific Party*, 1992], impacting morphologic interpretation. However, new data reveal sufficient basement exposures to show that the western basin comprises various morphologically distinct terrains, including abyssal hill fabric with corresponding magnetic lineations.

3.2.1 Abyssal Hill Terrain

North of 19ºS western basin seafloor largely consists of abyssal hill fabric. This fabric is characterized by N-S oriented ridges and valleys, some reaching 100 km in length. In this narrow part of the western basin (approximately 50-100 km wide), the abyssal hill fabric is found in close proximity to the Lau Ridge and extends eastward to the pseudofault (*Figure 3.3*). South of 19ºS much of the terrain adjacent to the Lau Ridge has a flat smooth appearance, due to sedimentation, imaged in seismic reflection profiles [*Parson et al.*, 1992; *Parson et al.*, 1994]. In places, the crests of linear abyssal hills stand above the sediments.
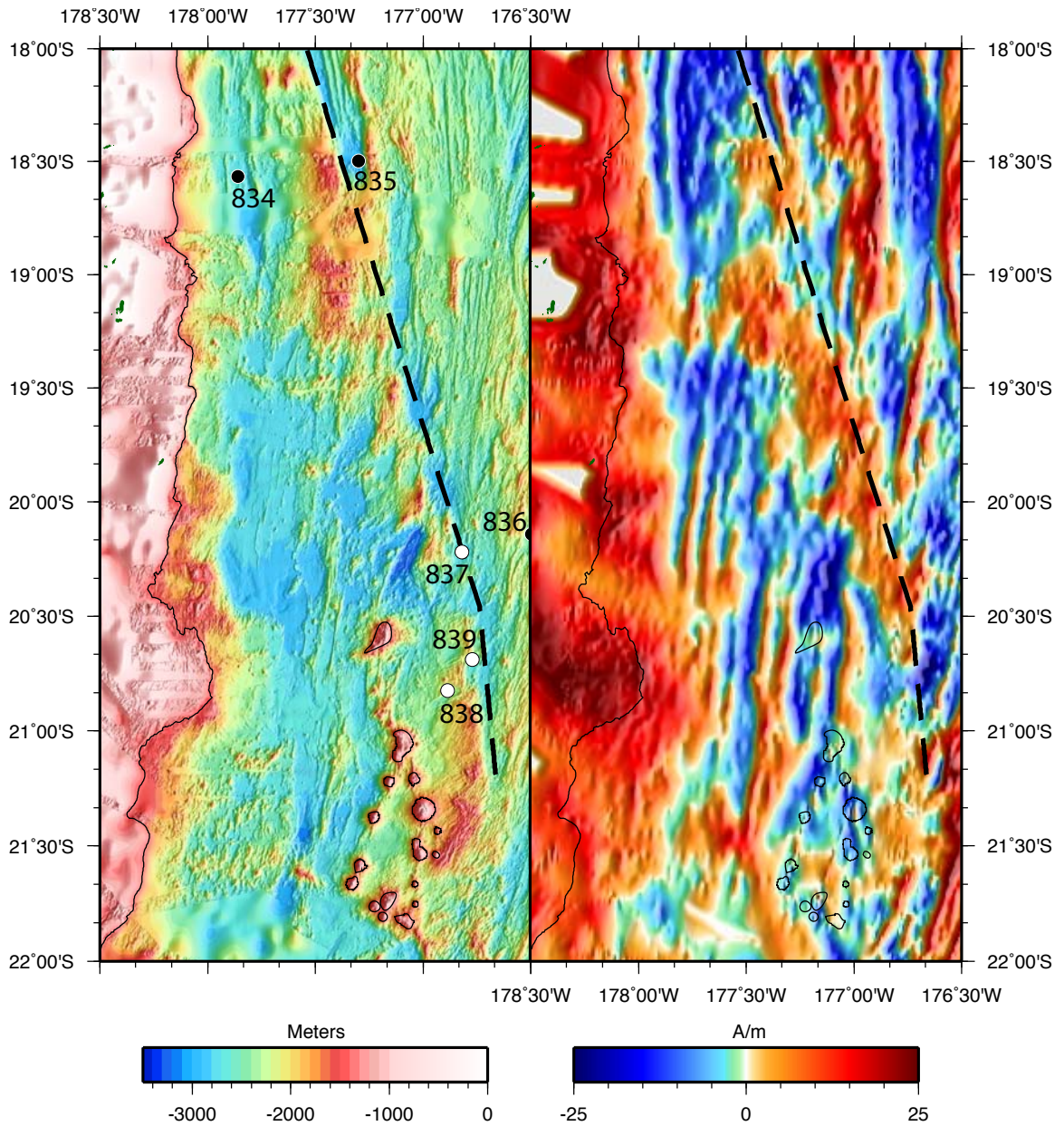
Figure 3.3. Bathymetry (left) and magnetization (right) of the western Lau Basin. The pseudofault is represented by a dashed black line, and subaerial features are in dark green. The Lau Ridge and western basin seamounts are outlined with simplified 1,450-m contours. ODP drill sites are shown on the bathymetry map, with MORB-like lavas represented by black dots and transitional or arc-Like lavas represented by white dots [*Hawkins*, 1995].

Farther east, ridges are more prominent, occasionally exceeding 50 km in length and cresting at depths near 2,000 m. South of ~21°30'S clear abyssal hills are not evident,

however, data also become sparser. Abyssal hill terrain has similarly oriented linear

magnetization anomalies on the order of ±15 A/m, with sharp east-west boundaries. To

the north and south, however, some of these anomalies taper beyond the apparent ends of

the ridges. Some lineations, as relative variations in amplitude, continue into areas where

the overall level of magnetization becomes negative. Most positive anomalies are found

in offset pairs, but near 20º30'S a series of up to 6 parallel positive lineations can be seen.

The southern terrain generally corresponds to low acoustic reflectivity, though

sharp lines of slightly high reflectivity can be found corresponding to some of the more

prominent ridges. ODP Site 834, located in the northern terrain, is primarily characterized

by mafic MORB (Mid-Ocean Ridge Basalt)-like lavas [*Hawkins and Allan*, 1994].

Basement ages range from 3.8 Ma to greater than 5.5 Ma with depth, and the initiation of

volcanism is estimated at 6 Ma. Sedimentation from the Lau Ridge is apparent [*Parson*

and Hawkins, 1994].

3.2.2 Ridges and Knolls Terrain

At various locations adjacent to the Lau Ridge a different, hummocky terrain is

found. Three of these areas are apparent in the current mapping: near 19ºS, near 21º30'S,

and a smaller area near 17ºS. The locations also correlate with local bathymetric swells or

groups of seamounts near the pseudofault and the eastern platform described below. This

terrain has a weak N-S oriented fabric, which is superimposed by small conical to

elongate edifices. Ridges are typically 5 to 15 km in length, while knolls are generally <2

km in diameter. Both ridges and knolls rarely crest shallower than 1,800 m though some

reach ~1,500 m while surrounding seafloor is ~2,500 m. This terrain displays a broad,

weak magnetization pattern, generally within ±10 A/m. The character is very dissimilar

from the adjacent Lau Ridge or neighboring abyssal hill fabric. While average acoustic reflectivity in this region is low, some features correspond to discrete points of high reflectivity. Similar "ridges and knolls" terrain was described in the Havre Trough [*Fujiwara et al.*, 2001; *Wysoczanski et al.*, 2010], and at the southern end of the VFR [*Martinez and Taylor*, 2006; *Watanabe et al.*, 2010].
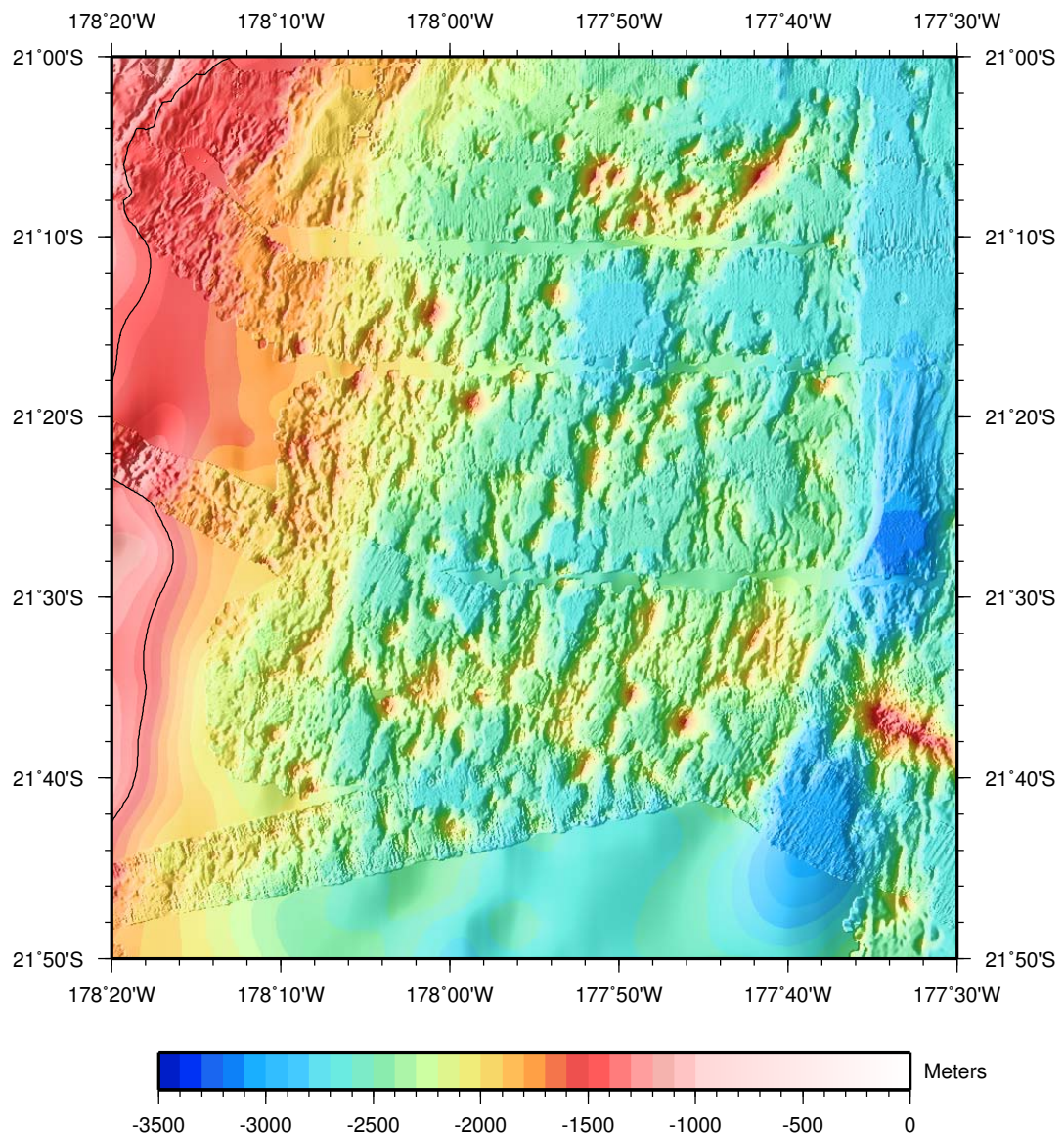
Figure 3.4. Bathymetry of the western Lau Basin "ridges and knolls" terrain. The eastern margin of the Lau Ridge is highlighted with a 1,450-m contour.

3.2.3 Eastern Platform

An irregular platform is found along the eastern edge of the western basin, adjacent to the pseudofault (*Figure 3.3*). From crests near 1,400 m in places, the western margin of this platform slopes gradually to the basin floor, while the eastern margin is sharp, and the seafloor quickly deepens. This platform appears to have N-S to NE-SW oriented striations or canyons intersecting it, typically varying with the orientation of the pseudofault. Seismic reflection profiles indicate this domain is sedimented, but that basement is irregular and possibly block faulted or stepped [*Parson et al.*, 1994]. It is shallower and wider opposite the areas comprising ridges and knolls terrain.

This area occasionally overlaps with a broad, weak, positive magnetic anomaly <15 A/m. ODP Sites 837, 838, and 839 were along this eastern platform [*Hawkins and Allan*, 1994; *Hawkins et al.*, 1994]. The single igneous unit retrieved at Site 837 is intermediate, containing basaltic andesite. Site 838 returned large amounts of volcaniclastic sediments, but no basement rock. Multiple units of basement rock were retrieved at Site 839. They are transitional, ranging from mafic to intermediate and comprising both basalt and basaltic andesite. The oldest overlying sediments for all three sites are late Pliocene in age (about 2 Ma), but no basement rock is dated. Few dredges have sampled the western basin, but four dredge sites along the eastern platform also returned arc-like or transitional lavas [*Hawkins*, 1995].
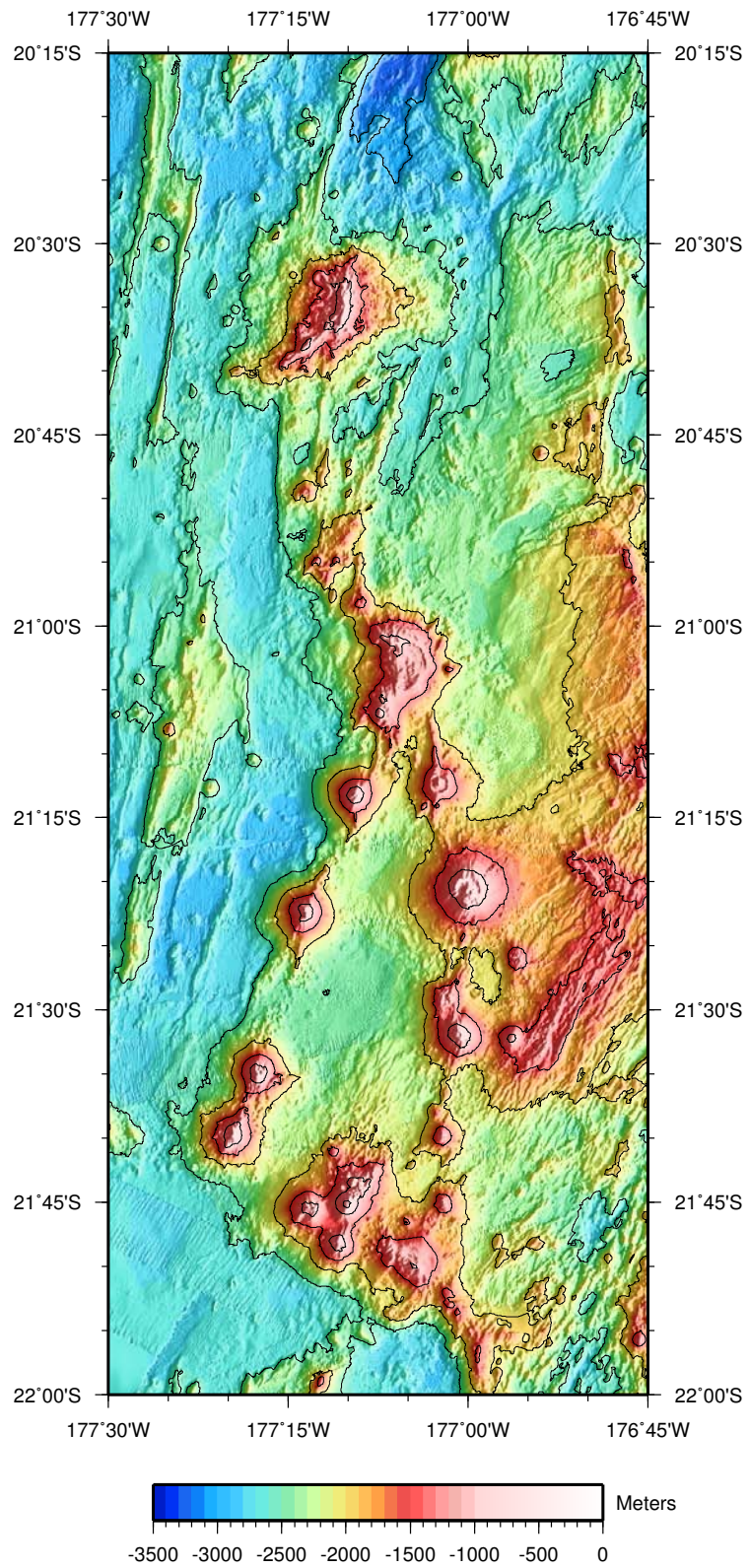
Figure 3.5. Contoured bathymetry of seamounts in the western Lau Basin. The contour interval is 500 m.

3.2.4 Western Basin Seamounts

To the southeast, as the western basin widens to roughly 150 km, there is an array of seamounts. Many of these seamounts shoal to depths of 1,000 m, some reaching 500 m, while diameters range from 5 to 20 km. Deeper ridges, oriented N-S to NE-SW, appear to connect the seamounts. The larger seamounts have small landslide scarps on their flanks. In general the seamounts are conical and young looking, however some appear to have resurgent domes within collapsed calderas. They are associated with magnetization anomalies that are often weak and vary between negative and positive polarity across a given seamount. These seamounts clearly correlate to discrete patches of high acoustic reflectivity. These patches continue to the northwest of the seamounts, though the terrain becomes flat. The patches form a trend subparallel to the pseudofault, offset by ~40 km.

3.3 Pseudofault

The pseudofault generally forms an approximately linear NNW-SSE trending bathymetric trough that separates the western basin from the central basin. It represents the western extent of crust formed along central basin spreading centers [*Hey*, 1977]. In detail it is irregular and discontinuous, comprised of a chain of sub-basins up to 2,800 m deep, trending in approximately a 165°/345° orientation. The pseudofault trough generally forms a steep escarpment bounding the shallower platform to the west. To the east, N-S oriented abyssal hill fabric is subparallel to the basins. The southern tips of abyssal hills often separate the pseudofault basins. At 18°45'S, a pseudofault basin truncates in the shallow platform terrain and is apparently replaced by another

pseudofault to the east. Near 20°45'S, the trend of the pseudofault becomes more southward, and at 21°15'S it loses definition. The seafloor here quickly shallows to ~1,500 m and farther south, the basins are replaced by ridges and knolls terrain. South of 22°10'S fabric becomes chaotic and there is no clear boundary between the western and central basins.

The pseudofault does not have a clear magnetization pattern, but it can be identified as a transition between different patterns and trends. To the west the magnetization is broad and weak over the shallow platform, while stronger, linear anomalies are found to the east. The sub-basins appear magnetically continuous with the shallow platform, displaying broad, weak magnetization. Similar to morphology, magnetization patterns also lose definition to the south with no clear lineations between the pseudofault and the positive anomaly encompassing the axis. ODP Site 835 is located on the eastern edge of the pseudofault [*Hawkins and Allan*, 1994; *Hawkins et al.*, 1994]. It is due east of Site 834, on the opposite side of the shallow platform bounding the western basin, and is similarly mafic and MORB-like. The single igneous unit retrieved gives a minimum basement age estimated at 3.2 Ma. While dredge sites immediately west of the pseudofault have typically returned arc-like or transitional lavas, those in the pseudofault basins and immediately to the east have returned MORB-like lavas [*Hawkins*, 1995].
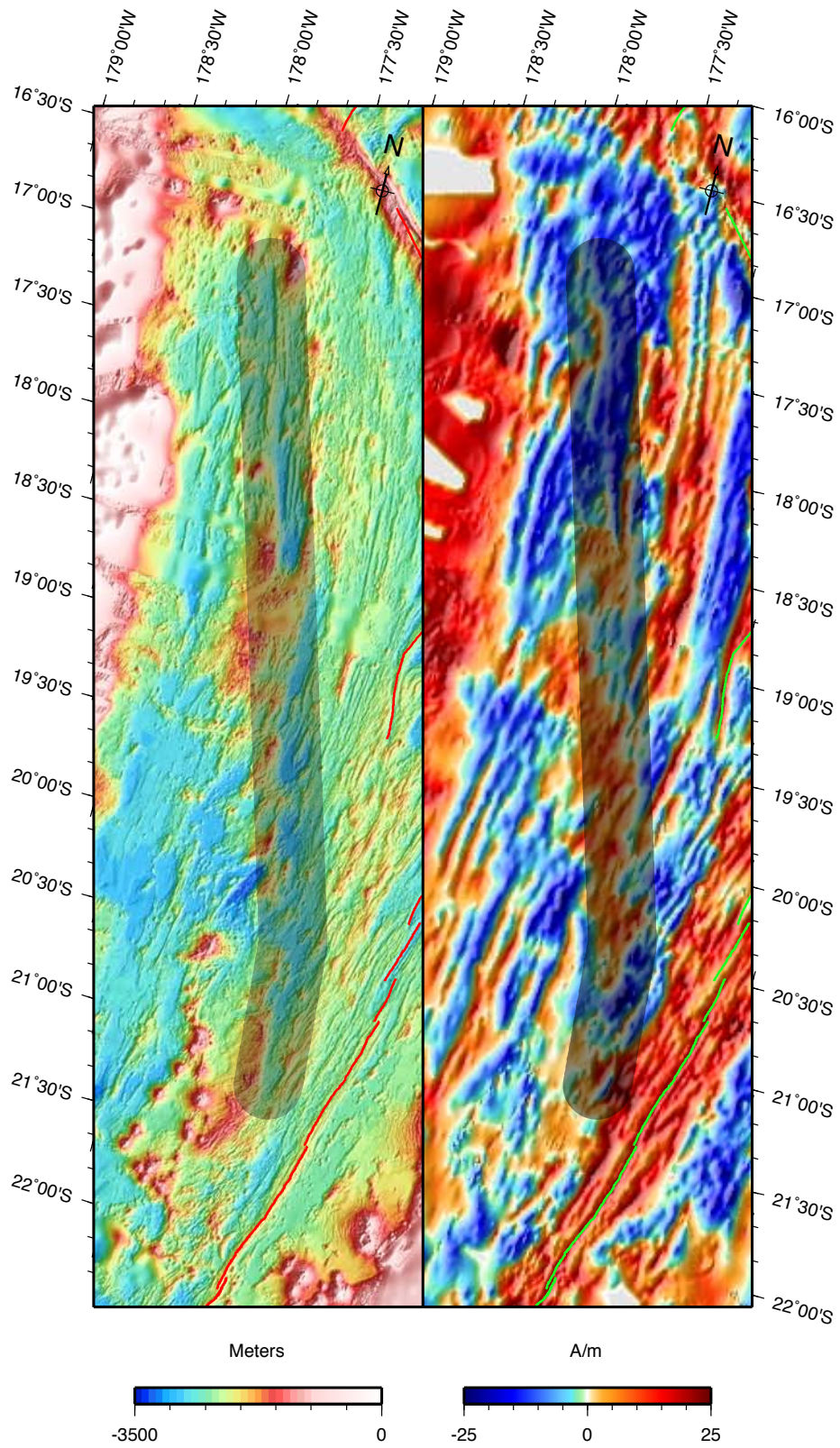
Figure 3.6. Bathymetry (left) and magnetization (right) of the pseudofault separating the western basin from the central basin. The pseudofault is

highlighted with dark gray. Plate boundaries are indicated with red on the bathymetry map and light green on the magnetization map.

3.4 Central Basin

Active spreading centers are found within the central basin. From north to south these are the Lau Extensional Transform Zone (LETZ), the Central Lau Spreading Center (CLSC), the Intermediate Lau Spreading Center (ILSC), the East Lau Spreading Center (ELSC), and Valu Fa Ridge (VFR) (*Figure 3.1*). The Peggy Ridge, a transform boundary, is found northwest of the LETZ. South of the Peggy Ridge, all offsets are non-transform. The LETZ transitions between the Peggy Ridge and the CLSC. The short ILSC is offset to the east, overlapping adjacent spreading centers, and the ELSC is offset eastward again. The VFR is very slightly offset from the ELSC and is primarily distinguished by a change in morphology.

The central basin almost entirely comprises roughly N-S oriented fabric. This includes typical abyssal hill fabric characterized by continuous linear ridges, as well as more discontinuous, shallower fabric comprising arcuate ridges. Both types fan out toward the north, as the basin widens. The linear fabric corresponds to intense N-S oriented magnetic anomalies with sharp boundaries. These anomalies are more developed than those in other parts of the basin, and this crust appears similar to that formed at mid-ocean ridges [*Taylor et al.*, 1996]. To the south, these anomalies both narrow and become fewer in number, as the basin narrows. Petrology varies, with silica content increasing in the direction of propagation [*Hawkins*, 1995; *Langmuir*, 2010]. Most seismicity within the basin ranges between strike-slip and tensional, but very little is recorded along the active spreading centers [*Ekström*, 2011]. While along-axis features have been well

studied [*Dunn and Martinez*, 2011; *Martinez and Taylor*, 2002; 2003; *Martinez et al.*, 2006], we focus primarily on off-axis regions.
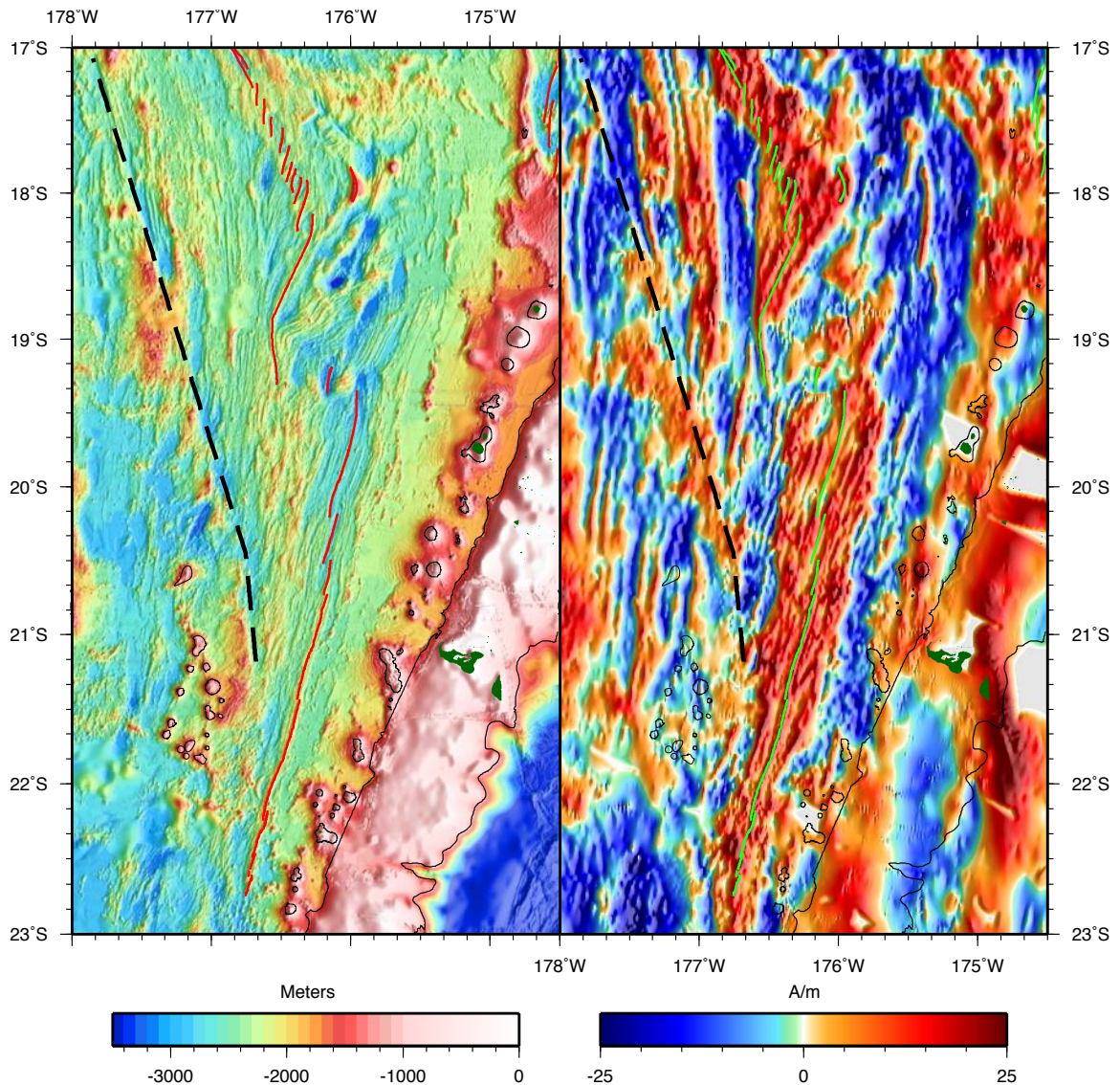
Figure 3.7. Bathymetry (left) and magnetization (right) of the central Lau Basin. The pseudofault is represented by a dashed black line, and subaerial features are in dark green. Tofua Arc volcanoes are outlined with 800-m contours, while other features are outlined with simplified 1,450-m contours. Plate boundaries are indicated with red on the bathymetry map and light green on the magnetization map.
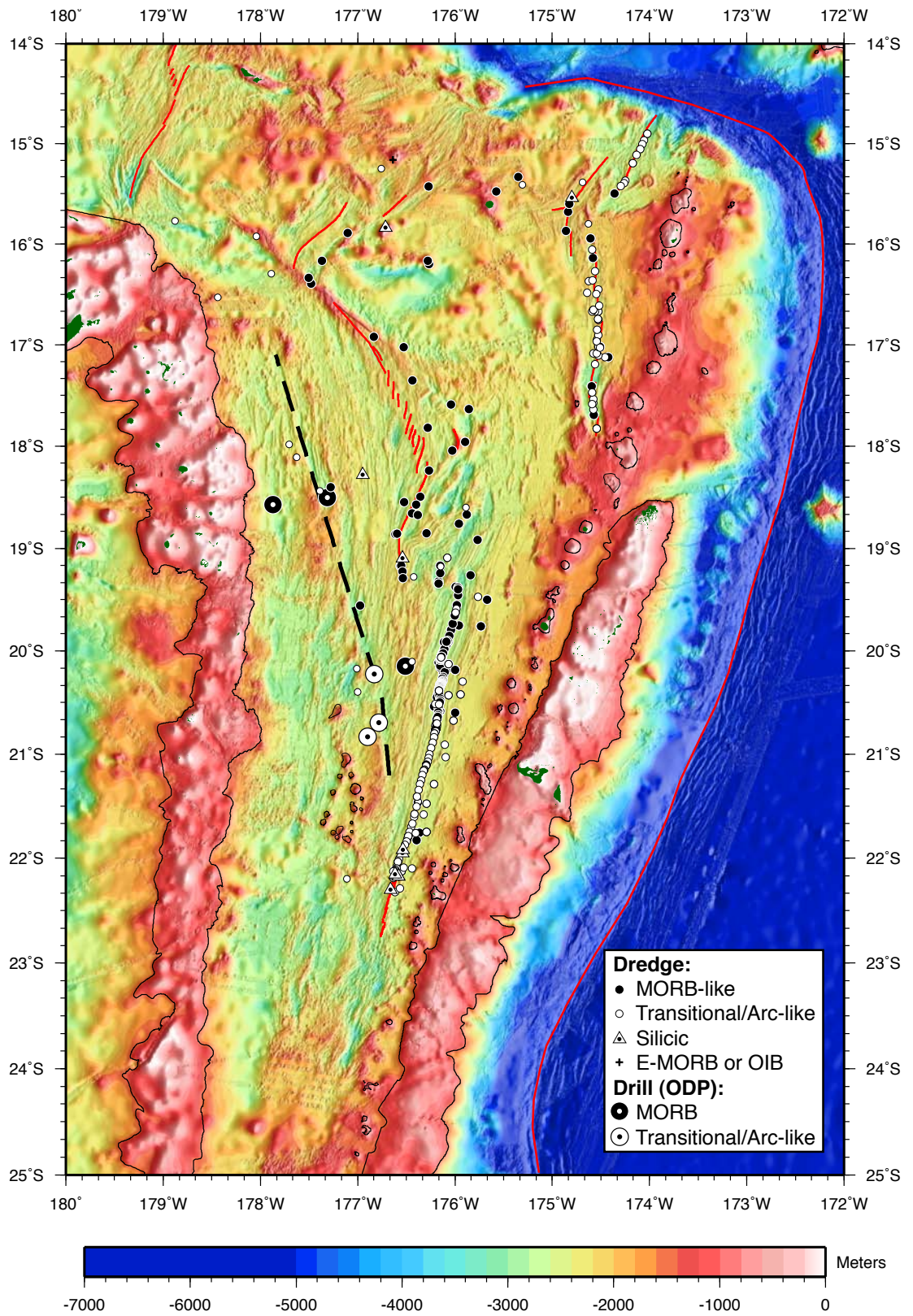
Figure 3.8. Bathymetry overlain by petrology from dredge and drill sites throughout the basin. Petrologic analysis is from Hawkins [1995], Keller et al.

36

[2008], and Langmuir [2010]. Symbols other than petrologic distinctions are as in Figure 1.3.
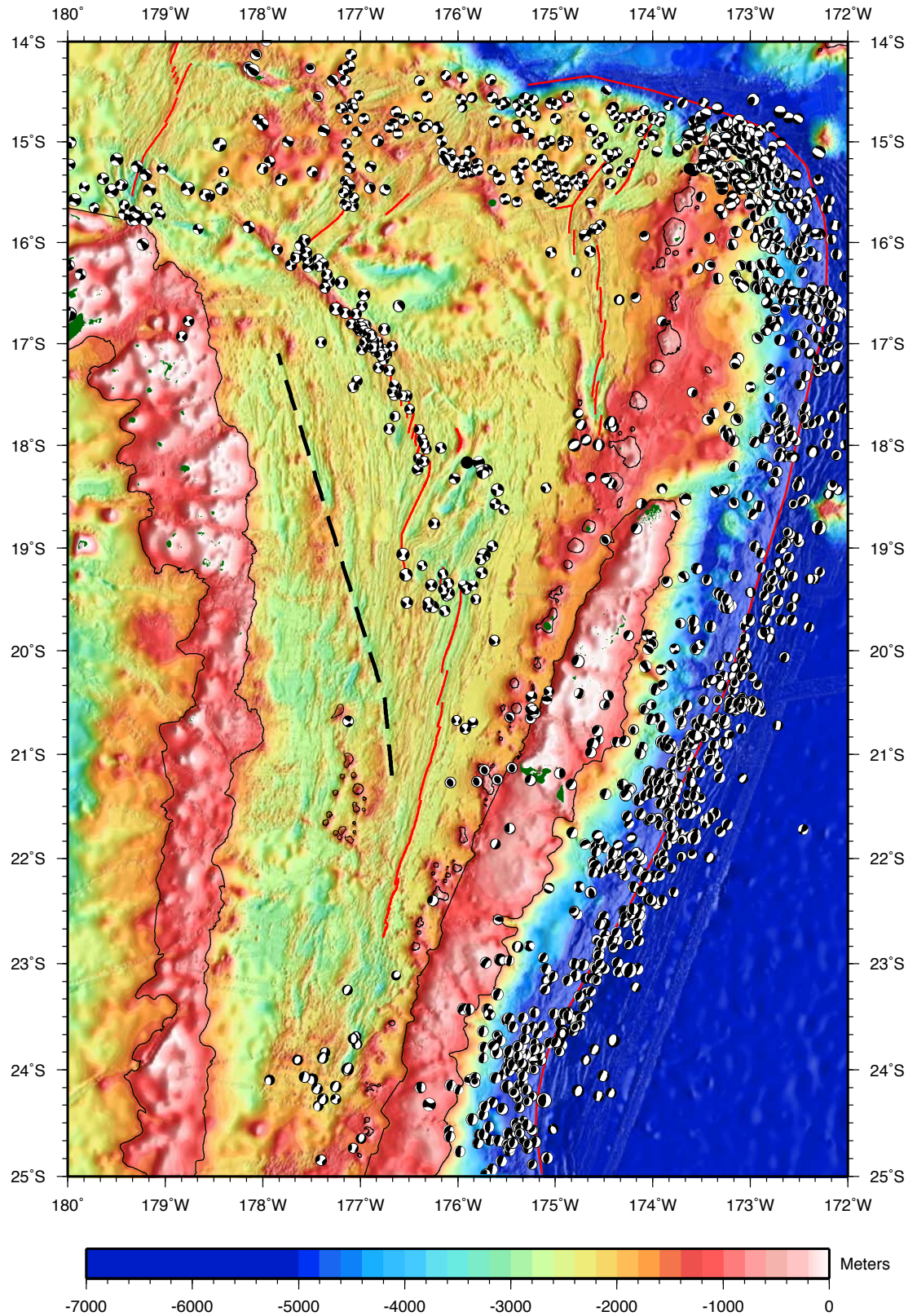
Figure 3.9. Bathymetry overlain by earthquake focal mechanisms. Focal mechanisms are from the Global CMT catalog [*Ekström,* 2011] and include earthquakes <50 km deep with magnitude >5.0. Symbols other than focal mechanisms are as in Figure 1.3.

3.4.1 CLSC, LETZ

The seafloor along the LETZ consists of many short, sinuous, en echelon ridges. To the north they are oriented N-S, and they gradually rotate to NNE-SSW towards the CLSC. The CLSC is a longer (~150 km), similarly oriented axial high that curves to a N-S orientation at both ends. Adjacent to this ridge, there are shorter parallel ridges with deeper highs. The positive anomaly encompassing active spreading centers (up to 25 A/m) narrows dramatically, from near 100 km along the LETZ to less than 10 km at the southern tip of the CLSC due to southward propagation [*Parson et al.*, 1990]. Along axis dredges have returned MORB-like lavas, with the exception of one, which returned silicic lavas [*Hawkins*, 1995]. The LETZ and CLSC are characterized by a broad band of high acoustic reflectivity [*Zellmer and Taylor*, 2001]. While the Peggy Ridge has a record of strike-slip earthquakes, the LETZ transitions north to south from strike-slip to slightly tensional, and seismicity along the CLSC is sparse [*Ekström*, 2011].

Off-axis mapping on the flanks of the LETZ and CLSC is primarily comprised of shallow-towed HMR1 phase bathymetry data and is therefore lower resolution [*Zellmer and Taylor*, 2001] than multibeam data, but terrains and features are well resolved (*Figure 3.7*). The seafloor west of both the LETZ and CLSC is formed of relatively uniform abyssal hill fabric. To the immediate west it drops to 3,000 m before gradually shoaling away from the axis. Ridges lengthen as well, exceeding 100 km in places. Adjacent to the pseudofault, ridges crest near 1,800 m depth and shorten to ~50 km. All

ridges in this region trend NNW-SSE, subparallel to the pseudofault. Magnetic anomalies in this region are intense (sometimes greater than ±20 A/m), and linear, corresponding to abyssal hill fabric. One dredge adjacent to shallower terrain in this region returned silicic lavas.
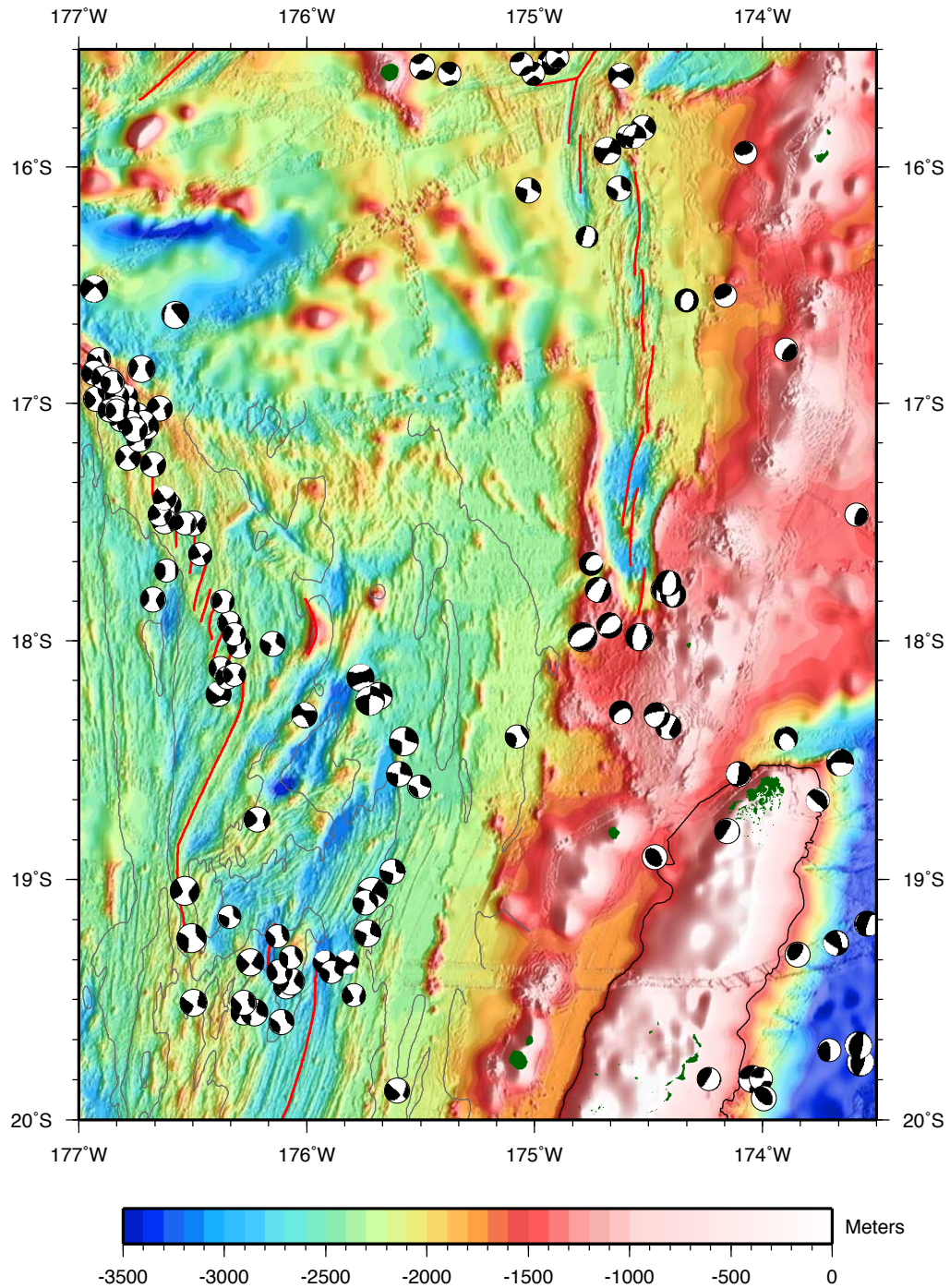
Figure 3.10. Bathymetry of the region of deformation east of the CLSC. Plate boundaries are in red, subaerial features are in dark green, and the Tonga ridge is outlined with a simplified 1,450-m contour. Fine gray lines indicate the 0-A/m contour of the magnetization inversion and focal mechanisms are as in Figure 3.9.

The area east of the CLSC comprises transferred lithosphere and extinct spreading segments of the ELSC. It forms irregularly trending abyssal hills and basins. Continuous ridges of transferred lithosphere display bends as great as 90°. There are also many sedimented, flat-bottomed basins, >3,000 m in depth, at the ends of ridges. Some of these are more elongate, while others are roughly circular with diameters of 15-30 km. Much of this area is characterized by positively magnetized crust (<15 A/m), but anomalies are non-linear. Rotated fabric may impede resolution of magnetic anomalies in this region. Dredges have returned a combination of MORB-like and arc-like or transitional lavas [*Hawkins*, 1995]. Recorded off-axis earthquakes surrounding this area are primarily strike-slip in nature [*Ekström*, 2011]. Some of these earthquakes are recorded in the non-transform offset between the southern tip of the CLSC and the northern tip of the ELSC. This seismicity is evidence for bookshelf faulting associated with southward propagation of the CLSC [*Wetzel et al.*, 1993]. North of 18°S, the fabric loses definition, with few discontinuous ridges maintaining a N-S orientation. To the east, nearing the Tofua Arc, fabric is more linear but also appears heavily sedimented. Few ridges crests stand above the sediments.

3.4.2 ELSC

Along the northern ELSC, the seafloor is greater than 2,500 m deep, and relatively flat with modest abyssal hill relief. South of 20°10'S, this flat region narrows

and is flanked by shallower seafloor. South of 20°30'S, the deep, flat terrain transitions to a broad axial high, before eventually being replaced by the peaked high of the VFR. Magnetization along the ELSC is generally intense and positive (up to 25 A/m). The central anomaly narrows southward with proximity to the opening pole [*Zellmer and Taylor*, 2001], from ~80 km to ~55 km. Adjacent to the ELSC there are some areas of weakly magnetized, negative polarity crust within the positive central anomaly. These areas typically correlate to bathymetric lows with weak and irregular abyssal hill fabric that may be associated with rotated seafloor. There is a ~5 km band of high acoustic reflectivity along the ELSC that decreases off axis. Lavas dredged along the northern ELSC are typically MORB-like, with SiO_2 content increasing southward, in the direction of propagation [*Hawkins*, 1995]. South of 21°45'S, nearly all along-axis lava samples have SiO_2 content greater than 52%.

Off axis, to the west of the ELSC, seafloor fabric is comprised of N-S oriented ridges, marginally similar to abyssal hill fabric. This terrain differs, however, in that the ridges are often arcuate in shape and tens of kilometers in length, shorter than the more linear abyssal hills. The transition to this terrain is sudden, with seafloor abruptly shoaling to 2,200 m, while ridges crest near 1,500 m. Some of this shallow, off-axis crust is within the Brunhes, but terrain appears weakly magnetized (±10 A/m) outside of the Brunhes and anomalies are difficult to identify. ODP Site 836 is within this terrain. Some shallower units are transitional intermediate-mafic, while deeper rocks are more definitively mafic basalt [*Hawkins and Allan*, 1994]. Volcaniclastic sediments are abundant, and are identified as basaltic andesite. Ages of sediments bounding the volcanic units are estimated at 0.6 Ma. An adjacent dredge returned transitional or arc-

like lavas [*Hawkins*, 1995]. Farther off axis, near the pseudofault, a small area of typical abyssal hill fabric is found. Ridges and magnetic anomalies here are continuous with off-axis fabric west of the CLSC, to the north.

East of the ELSC the seafloor flattens with few discontinuous, crescent ridges rising above surrounding sediments. South of 21ºS, continuing on the eastern flank, discrete knolls replace the arcuate fabric. Discrete patches of high acoustic reflectivity, more densely spaced than the knolls, characterize this region. This flat terrain appears heavily sedimented with volcaniclastics from the nearby Tofua Arc, and continues eastward until landslide scarps of the arc volcanoes are apparent. Magnetic anomalies are weak (±10 A/m) and difficult to resolve. Dredges in this region returned both MORB-like and transitional or arc-like lavas (*Figure 3.9*).

3.4.3 VFR

The VFR forms a peaked axial high, and has a very narrow region of abyssal hill fabric flanking its northern section. Terrain is generally flat off axis, but has some crescent ridges <20 km long to the immediate west. Farther off axis to the west, the southern end of the pseudofault transitions to ridges and knolls terrain similar to that found in the western basin. To the east of the VFR the terrain is flat, with sparse knolls, continuous with the ELSC associated terrain to the north. Near the southern end of the VFR, these knolls are replaced by larger seamounts that reach ~1,500 m, with diameters <5 km. Along the VFR, only one positive magnetic anomaly (30-55 km wide) can be identified. It is more intense at the edges, nearing 25 A/m. The Brunhes anomaly reaches a minimum width of ~25 km before departing from the trend of southward narrowing as the opening pole is approached.
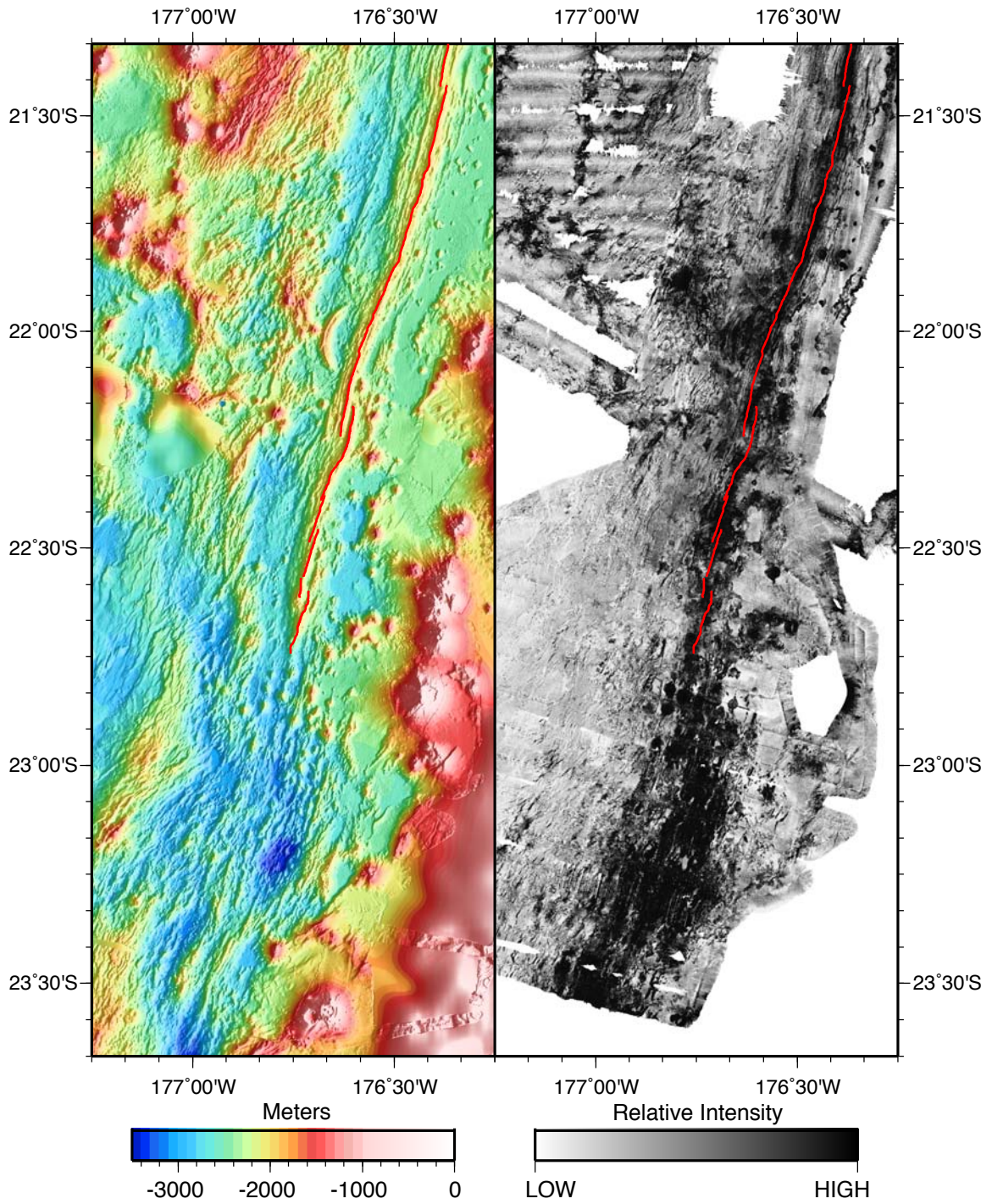
Figure 3.11. Bathymetry (left) and acoustic reflectivity (right) of the VFR (red line). South of the VFR, there is no identified locus of organized spreading.

Moving southward, as the axis nears the arc the sharp axial band of high acoustic reflectivity becomes less apparent. Numerous scattered, discrete zones of high reflectivity

can be found along and off axis, corresponding to knolls and arcuate ridges, especially the large crescent ridge west of the axis, near 22ºS. Most lavas in this region are arc-like or transitional [*Hawkins*, 1995; *Langmuir*, 2010]. Some are silicic in nature, and SiO_2 content often exceeds 60%.

South of the VFR, the axial high gives way to deeper seafloor (2,800 m) with ridges and knolls cresting near 1,800 m and basins exceeding 3,000 m. A positive magnetic anomaly continuous with the VFR remains intense, but becomes more irregular in width and character. To the west of this deep region, seafloor shallows to 2,000 m. Fabric in this region is oriented NE-SW and often sinuous, and a broad band of high reflectivity is apparent. There are a number of tensional earthquakes recorded near 24°00'S [*Ekström*, 2011]. This is the highest concentration of tensional seismicity in the basin.

3.5 Northern Basin

North of the Peggy Ridge, the basin continues to widen before terminating in a boundary with the Pacific Plate. The northern basin is dramatically wider than the southern basin, indicating much faster overall opening rates occur in the north. This faster opening is accommodated by multiple spreading centers, including the Futuna Spreading Center (FSC), Northwest Lau Spreading Center (NWLSC, Fonualei Rift and Spreading Center (FRSC) and Northeast Lau Spreading Center (NELSC) [*Pelletier et al.*, 1998]. Predicted bathymetry from satellite altimetry data indicates the terrain between the identified spreading centers is tectonically complex. Limited shipboard data is too sparse for adequate interpretation, but indicates that shallow terrain and seamounts are abundant

while abyssal hill fabric is minimal. Lavas in the northeast Lau Basin, along the FRSC and NELSC are predominantly >52% SiO_2. Arc-distal areas, including the northern FRSC and the Mangatolu Triple Junction are more MORB-like [*Hawkins*, 1995; *Keller et al.*, 2008; *Langmuir*, 2010]. Off-axis seismicity is high in this region, ranging from compressional in the northeast corner of the basin to primarily strike-slip across the remainder of the basin [*Ekström*, 2011]. Few plate boundaries have been fully identified in this region, though microplate tectonics have been proposed based on seismic data [*Conder and Wiens*, 2011].

3.6 Tofua Arc

The Tofua Arc volcanoes form a chain parallel to the Tonga Ridge, along the eastern edge of the Lau Basin. They are often found in clusters and rise from flat seafloor ~1,800 m deep. Many shoal to depths less than 500 m, while some form islands. The larger seamounts generally display landslide scarps on their flanks. Those with mapped summits often exhibit collapsed calderas. North of 18°30'S, the region of flat seafloor encompassing the arc widens and shallows to 1,400 m, forming a broad (>100 km) platform, replacing the much shallower (~500 m) forearc platform of the Tonga Ridge. Shipboard mapping in this area is sparse, leaving the character of this terrain difficult to resolve. Magnetics data across the Tofua Arc is sparse, and primarily comprised of older aeromagnetic surveys [*Cherkis*, 1980]. In the few areas with shipboard mapping, the magnetization pattern is generally <15 A/m, broad, and positive, similar to the Lau Ridge.

The platform to the north of Vavaʻu may be moving independently of the Tonga Plate to the south. Geodetic data from Niuatoputapu indicates that while its motion relative to Australia is similar to that of Vavaʻu and Tongatapu, its motion relative to Vavaʻu and Tongatapu has a northward component of ~14 mm/yr [*Phillips*, 2003]. Vavaʻu and Tongatapu, however, are stable relative to each other. Thus the area north of Vavaʻu and between the Fonualei Ridge/NELSC and the trench may constitute a separate microplate.

3.7 Tonga Ridge

The Tonga Ridge bounds the eastern edge of the Lau Basin south of ~18°30′S and islands exhibited are primarily limestone. Limited igneous exposure on ʻEua, however, is late Eocene in age [*Ewart and Bryan*, 1972; *Hawkins and Allan*, 1994], similar to the Lau Ridge. The ridge is very sparsely mapped, so most observations are based on predicted bathymetry from satellite altimetry data. The NE-SW oriented ridge rises from sedimented seafloor surrounding the Tofua arc volcanoes along a sharp and linear margin. It forms a broad, flat plateau (50-100 km wide) that both forms islands and is cut by channels. North of 21º30'S it is generally less than 200 m in depth, exhibiting numerous islands including the main islands of Tonga. South of 21º30, the platform is approximately 500 m deep with some canyons <30 km in length and ~2,000 m deep cutting in from its eastern margin. At 23ºS, the ridge bends slightly southward and the sharp western margin becomes more irregular. The eastern flank is irregular and gradually deepens toward the Tonga Trench.

46

47
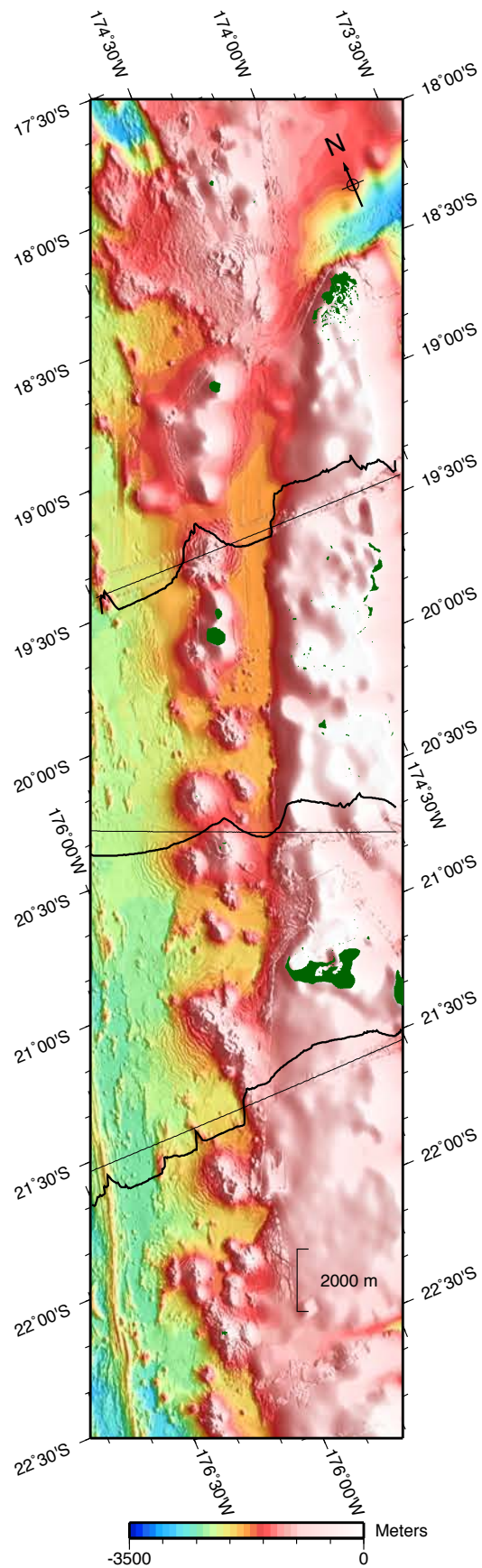
Figure 3.12. Bathymetry of the western Tonga Ridge margin. Cross sections sampling the bathymetry are displayed with thick black lines, while 1,500-m baselines are displayed with fine black lines. Cross section orientations are based on the limited ship tracks that continue on to the ridge. The transition from ridge to basin is uniformly sharp.

As noted above, the character of the ridge changes north of 18°30'S. The seafloor drops off into an E-W oriented canyon 2,500 m deep before rising to the 1,400-m plateau beneath the Tofua Arc. Similar to the Lau Ridge, the Tonga Ridge is generally too shallow for proper 3-D resolution of magnetic data as track line spacing becomes much wider than the water depth. Sparse data indicate the Tonga Ridge has a broad and strong positive magnetization pattern, up to 30 A/m.

3.8 Tonga Trench

The Tonga Trench, parallel to the Tonga Ridge, is oriented NE-SW. It reaches depths greater than 9,000 m and is near 11,000 m at its deepest. Along the northeast corner of the Lau Basin, the trench gradually curves west. East of the trench, there are trench-parallel escarpments from faults created by bending of the subducting Pacific Plate. Rare shipboard surveys do not reveal a clear magnetization pattern along the trench. The trench generally forms a boundary between positively magnetized crust within the basin and negatively magnetized crust on the subducting Pacific Plate, though magnetic field data are very sparse. Compressional seismicity is abundant along the Tonga Trench, both east and west of the boundary [*Ekström*, 2011]. It is especially abundant where the trench curves westward.

4. Discussion

Both the western and central parts of the basin express heterogeneous crustal accretion as detailed by new data collected throughout the basin. Distinct morphologic phases along the flanks of the ELSC include an initial phase that formed deep abyssal hill fabric adjacent to the pseudofault; a middle, more complex and robust phase where short, arcuate ridge segments formed along an axis close to the volcanic front; and a younger, less robust phase characterized by an overall flat seafloor with abyssal hill fabric [*Martinez and Taylor*, 2002]. Some of these sudden transitions show a clear correlation to arc proximity, indicating abrupt changes within the mantle wedge as subduction influence changes [*Dunn and Martinez*, 2011].

The western basin has similarly variable terrain, indicating that a range of processes occurred during early basin formation. While evidence for rifting is found along parts of the eastern Lau Ridge margin, linear magnetic anomalies and abyssal hill fabric within the western basin support seafloor spreading initiating early in the basin's opening history. Similarly, arc-like volcanoes and a shoaling platform along the eastern margin of the western basin imply that this region formed as a backarc basin before the locus of spreading migrated eastward.

Although we interpret a magmatic origin for most of the western basin, this does not imply exclusively organized seafloor spreading. In addition to clear abyssal hill fabric, previous studies have identified regions of ambiguous seafloor comprising small volcanic ridges and knolls in parts of the Lau Basin and Havre Trough. Seismic reflection data and dredge samples indicate that these features are volcanic intrusions with MORB-like compositions [*Fujiwara et al.*, 2001]. Further studies show that south of the VFR,

49

this "ridges and knolls" terrain characterizes the volcanically active area where organized spreading transitions to a broad volcano-tectonic zone [*Martinez and Taylor*, 2006; *Watanabe et al.*, 2010]. Within the Havre Trough, this terrain is identified within neo-volcanic regions [*Wysoczanski et al.*, 2010]. These currently active areas support the interpretation that a form of diffuse spreading creates these "ridges and knolls" terrains. While it has been previously interpreted as rifted arc crust that has subsequently been injected with magma, there is no evidence to indicate that this crust is older than basin opening or associated with rifted arc material. Furthermore, the overall strength of magnetization is rather high, comparable to that of the VFR, indicating magmatism in this region is robust and magnetization is not simply the signature of a thin carapace of recent volcanics overlying older rifted crust. We further interpret inactive but morphologically similar terrains in the western basin as having formed by this method.

Our new compilation of bathymetric and magnetic data depict complex processes involved in backarc basin opening, including non-rigid plate kinematics, variable magmatic crustal production and organized and diffuse forms of seafloor spreading. The development of these processes is described in more detail in the following sections.

4.1 Lau Ridge

The variable nature of the transition from the Lau Ridge to the basin floor demonstrates that multiple processes were active during the initial opening stages of the Lau Basin. Steep slopes along much of the eastern margin of the Lau Ridge indicate an abrupt thinning of pre-existing arc crust. Basin-floor terrain adjacent to these slopes often forms abyssal hills, supporting early initiation of seafloor spreading in the western basin

(*Figure 3.2*). In other locations, gentle or stepped slopes may indicate modest amounts of more distributed rifting stepping the arc massif down into the basin. In either case, by the point where the Lau Ridge descends to typical basin depths, further extension within the basin appears to be primarily accommodated by magmatic crustal accretion. The continuation of volcanism along the Lau Ridge during basin opening [*Whelan et al.*, 1985] indicates that the ridge was not immediately cut off from magma sources. As the locus of opening was in the forearc, arc-volcanic edifices were left behind on the soon-to-be remnant Lau Ridge. It appears that the reorganization of arc volcanism involved eastward migration across the nascent basin.

4.2 Western Basin

The western basin is characterized by multiple patterns of crustal accretion. Some of this accretion took place along western basin spreading centers, which were subsequently replaced by propagating ridges in the central basin. Abyssal hill fabric and linear magnetic anomalies (*Figure 4.1*, orange highlight) support an organized spreading interpretation for much of the western basin. While magnetic sequences have the character of seafloor spreading anomalies, they are short and offset from each other. This, in addition to possible overprinting by younger volcanism and propagation episodes, has impeded confident correlation of anomalies to the geomagnetic reversal sequence. Igneous basement recovered from ODP Site 834 within this terrain shows that organized spreading initiated by 5.5 Ma [*Parson and Hawkins*, 1994] (Chron 3r). Extensive representation of the Jaramillo reversal (~1 Ma) in the central basin indicates that the youngest western basin anomalies are perhaps the beginning of Chron 1r (~1.8 Ma).
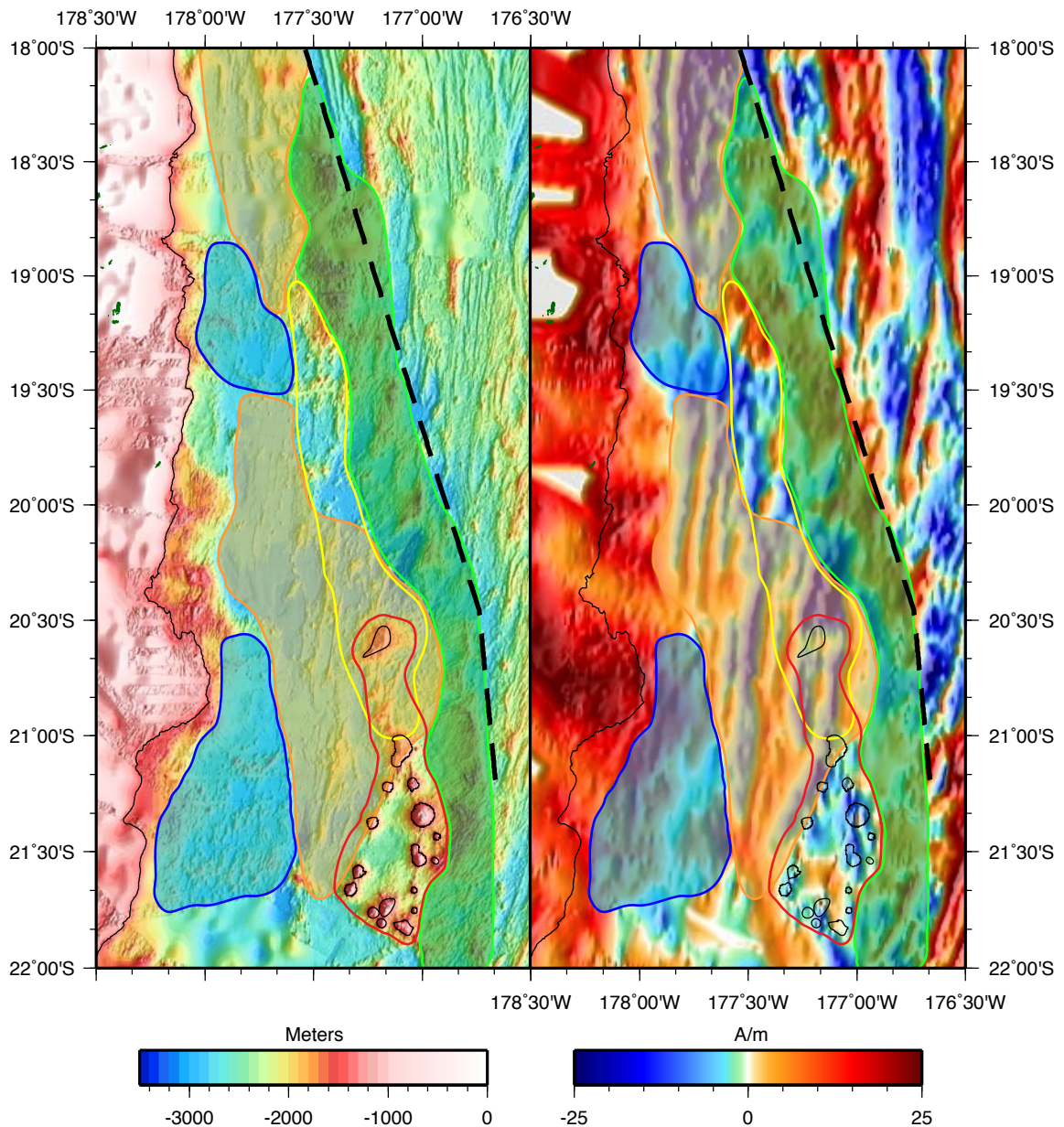
Figure 4.1. Terrains of the western Lau Basin. Underlying maps show bathymetry (left) and magnetization (right). The pseudofault is represented by a dashed black line, and subaerial features are in dark green. The Lau Ridge and western basin seamounts are outlined with simplified 1,450-m contours. Abyssal hill terrain is highlighted in orange, ridges and knolls terrain in blue, and the western basin platform in green. Seamounts are outlined in red, and patches of high backscatter are outlined in yellow.

Relict ridges and knolls terrain in the western basin (*Figure 4.1*, blue highlight) is interpreted to form through diffuse crustal accretion, due to the morphologic similarity to presently forming terrain identified in the Havre Trough and south of the VFR [*Fujiwara et al.*, 2001; *Martinez and Taylor*, 2006; *Watanabe et al.*, 2010; *Wysoczanski et al.*, 2010]. This terrain is likely a region of broad volcanism though it has not yet been sampled within the western basin. Active examples of this terrain adjacent to the arc volcanic front indicate that arc-proximity may be a control on its formation. Other examples adjacent to the southern section of the pseudofault, where basin opening rates slow relative to the north, may indicate that spreading rate is also a control on formation of this terrain.

Seamounts in the western basin (*Figure 4.1*, red outline) may have developed as a small proto-arc, analogous to the current Tofua Volcanic Arc, though their composition is unknown. Larger seamounts may indicate an incipient stage of volcanic arc formation that was terminated by ELSC propagation and formation of the central basin. During western-basin opening, the proto-arc would have been east of the locus of spreading, and a part of the young Tonga Plate. As the ELSC subsequently propagated southward to form the central basin (to the east of the seamounts), these volcanic edifices were transferred to the Australian Plate. This process separated them from the eastward migrating trench and related magmatism, leading to the cessation of volcanism. Patches of high backscatter on flat seafloor northwest of the largest seamount (at 20°35'S, 177°10'W) may also be a remnant of this magmatism (*Figure 4.1*, yellow outline). This area may have been separated from magmatism earlier than the seamounts, preventing seamount formation. These patches may also represent a pseudofault bounding western

basin spreading, as they fall along the northeastern extent of abyssal hill fabric, though this does not explain their discrete nature.

Formation of the eastern platform (*Figure 4.1*, green highlight) could be due to one of many processes. One possible interpretation is that this crust is rifted Lau Ridge arc terrain, as evidenced by the block-faulted or stepped basement [*Parson et al.*, 1994]. While dredge and drill samples within this terrain are characterized as arc-like or transitional [*Hawkins*, 1995], overlying sediments are younger than the initiation of basin opening [*Hawkins and Allan*, 1994] so there is no direct evidence that sampled terrain directly reflects rifted Lau Ridge crust. A second interpretation is that this crust may be transferred lithosphere from propagation of the ELSC replacing western basin spreading centers, akin to the terrain in the non-transform offset between the propagating CLSC and the ELSC. Its appearance is inconsistent with a bookshelf faulting mechanism, and would therefore require another type of oblique shear mechanism. This interpretation, however, could account for the variable basement character and rifted appearance in seismic reflection profiles. A third explanation is that this terrain may have formed as a younger arc platform in conjunction with the proto-arc described above, akin to the raised terrain the Tofua Arc is built upon.

4.3 Pseudofault

The character of the pseudofault not only indicates southward propagation of central basin spreading centers; it provides information about the modes of spreading taking place throughout its history. Discontinuity along the pseudofault demonstrates that multiple axes formed over time, as evidenced by the numerous abandoned ridge tips and

sub-basins found along the pseudofault. Each of these axes was replaced by a subparallel axis, generally to the east. These axes may have had some difficulty propagating into the crust of the western basin platform. Initial opening of the central basin was predominately through organized seafloor spreading where the pseudofault is present.

The change in orientation of the pseudofault near 20°45'S, to a more southward direction, indicates an acceleration in propagation along the ELSC occurred. It is apparent that the nature of propagation changes further between 21°30'S and 22°S. The pseudofault loses definition before disappearing entirely, and is replaced by terrain similar to "ridges and knolls" terrain, signaling a transition to more diffuse crustal accretion. While organized spreading takes places along the southward propagating VFR, a defined pseudofault separating this crust from that of the western basin is absent in this region.

The steep eastern margin of the pseudofault is similar to the steep western margin of the Tonga Ridge suggesting they may be conjugate features, though there are some discrepancies with this interpretation. In addition to the more apparent discontinuity within the pseudofault, the pseudofault and the Tonga Ridge are not equidistant from the ELSC. Recent seafloor spreading is largely symmetric in nature, necessitating other asymmetric processes in the past, in addition to ridge propagation, which is not strongly supported by the magnetic data. However, estimating an eastern pseudofault that is equidistant from the axes produces an inconsistent boundary, that divides abyssal hill terrain from the arc platform to the south, but cuts through the arc platform and the Tonga Ridge further north (*Figure 4.2*), supporting an asymmetric spreading history. Both features contrast sharply with the more variable eastern margin of the Lau Ridge, though

this may be due to other inherent differences between the features, which are further

discussed below.
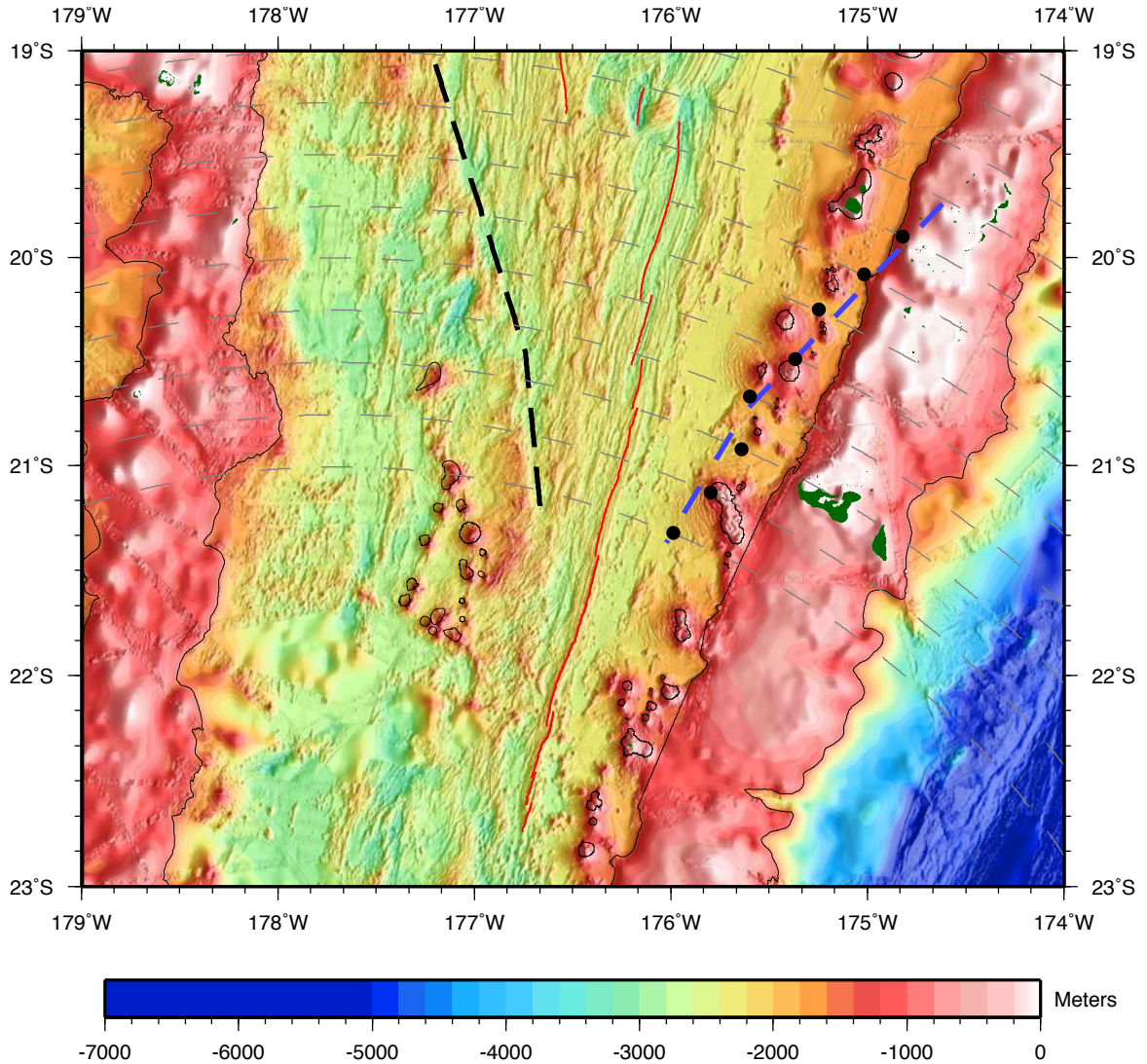
Figure 4.2. Bathymetry overlain by one estimate of the eastern conjugate of the pseudofault. The pseudofault to the west (dashed black line) and black dots to the east are equidistant from the axes along flow lines (dashed gray lines). Assuming symmetric spreading along the ELSC, the blue dashed line estimates where an eastern pseudofault would be. Other symbols are as in Figure 1.3. While this eastern pseudofault would separate the basin floor from the Tofua Arc platform to the south, further north it cuts through the platform and the Tonga Ridge, indicating, instead, that some asymmetric spreading may have occurred during central basin opening. This asymmetry is supported by the numerous abandoned ridge tips found along the (western) pseudofault—evidence that axes

have formed and been replaced by each other throughout the evolution of the central basin.

4.4 Central Basin

Recent studies along the currently active ELSC show that magmatic productivity along an organized spreading center is strongly controlled by arc proximity [*Dunn and Martinez*, 2011; *Martinez and Taylor*, 2002; 2003; *Martinez et al.*, 2006]. This indicates that irregular seafloor morphology throughout the basin can be explained by variations in magmatic processes rather than arc rifting. Similar to the western basin, the central basin is comprised of multiple patterns of crustal accretion. While crust is predominantly formed by seafloor spreading, this mechanism has at least three different expressions within the central basin, including typical abyssal hill fabric, more discontinuous arcuate fabric, and low relief abyssal hill fabric. Additionally, "ridges and knolls" terrain is common in more southern parts of the central basin. It is not clear how the earliest central basin crust is influenced by the arc-proximity trend. Difficulties determining the original arc proximity of this crust are further complicated by the migration of arc volcanism. This crust may have formed in the forearc region of the possible western basin proto-arc, before volcanism migrated further eastward. Crustal formation in this environment would have been dramatically different from that along other loci of spreading; occurring adjacent to the boundary formed by the Tonga Trench and away from mantle wedge regions where current spreading takes place.

4.4.1 CLSC, LETZ

While the Brunhes Chron along the CLSC and LETZ widens to the north, similar to the Brunhes Chron along the ELSC due to northward increasing opening rates, it further narrows southward due to propagation within the Brunhes Chron. The majority of off-axis terrain between the CLSC/LETZ and the pseudofault is interpreted to have formed along the ELSC before it was replaced [*Parson and Hawkins*, 1994]. The NW-SE orientation of this terrain west of the axes may be indicative of relict axis orientation, or it could instead represent other forms of reorganization such as a migrating pole. The transition between terrain oriented similar to the active axes and more continuous off-axis terrain coincides with a transition to deeper seafloor, similar to that found along the northern ELSC. The intermediate terrain gradually shoals toward the pseudofault, as seafloor age increases. Shallower terrain adjacent to the pseudofault originally formed much closer to the arc before being moved away by continued seafloor spreading, indicating arc-proximity influenced its formation. A dredge in this terrain returned silicic lava, demonstrating possible arc influence or fractionation, though the oldest central basin lavas found along the pseudofault are MORB-like within typical abyssal hill fabric. Longer, more continuous ridges off axis represent a continuous axis at the time of formation.

Terrain east of the CLSC and LETZ appears to have formed as typical abyssal hill fabric before being deformed and rotated by later ridge propagation processes. While a central Lau microplate encompassing this region has been suggested [*Conder and Wiens*, 2011], seafloor fabric indicates this terrain has not behaved in a rigid manner. This terrain was likely caught between the dying ELSC and the propagating CLSC, becoming

transferred lithosphere [*Kleinrock and Hey*, 1989]. As axis propagation has occurred, the region of non-transform offset between the southern tip of the CLSC and the northern tip of the ELSC has migrated southward. Bookshelf faulting evident in the current offset would have migrated as well [*Wetzel et al.*, 1993], further impacting the terrain. Farther to the east, seismologic, morphologic and acoustic reflectivity data do not support a well-defined Niuafoʻou-Tonga plate boundary between the southern tip of the FRSC and the CLSC/LETZ, though aseismic, diffuse deformation may occur.

4.4.2 ELSC, VFR

Distinct morphologic phases along the ELSC include an initial phase that formed deep abyssal hill fabric; a middle, more complex phase where short, arcuate ridge segments formed; and a younger phase characterized by an overall flat seafloor with abyssal hill fabric. Successively older phases would have formed along axes closer to the arc than their more modern counterparts, and more southern terrains would have formed closer to the arc due to the southward increasing arc proximity of the ELSC. While the oldest crust (adjacent to the pseudofault) is typical abyssal hill fabric, the arcuate, shallow fabric is likely arc-influenced, and the subsequent sudden transition to deep, flat abyssal hill fabric shows a clear correlation to arc-proximity, indicating abrupt changes within the mantle wedge as subduction influence changes [*Dunn and Martinez*, 2011].

Petrology along the axis also follows a pattern that correlates to arc-proximity. SiO_2 content increases southward; MORB-like lavas are found to the north end of the ELSC, arc-like or transitional lavas are found along much of the central section (within 75 km of the arc), and some silicic lavas are found to the south (~40 km from the arc). The transition between MORB-like and arc-like lavas also corresponds to the transition

from deeper terrain along axis to a broad axial high, while silicic lavas are found along the peaked axial high of the VFR.

The ELSC appears slightly offset within the Brunhes, lying east of center along the central sections. This indicates that spreading is asymmetric or that the axis has relocated. Apparently negative polarized crust adjacent to the ELSC (within the Brunhes Chron) may represent positively magnetized Brunhes era crust that was rotated by dueling propagation to the degree that it now appears negative. While this terrain is slightly off-axis, and not adjacent to any current segment ends, sinuous fabric indicates dueling propagation occurred.

The overall pattern of magnetization within the basin supports some form of asymmetry as well, with more anomalies being identified west of the axes. Ridge crests that stand above the sediments east of the axes have a sharper character than the arcuate ridges found west of the axes, supporting either an asymmetric spreading process or overprinting by younger magmatism after seafloor formed as abyssal hill fabric. However, the Tofua Arc may also overprint abyssal hill terrain, with younger lavas preventing resolution of magnetic anomalies while sediments disguise the original seafloor morphology. Terrain along the eastern edge of the Brunhes Chron shows a strong magnetic signature, but weak abyssal hill fabric, indicating this area is affected by sedimentation with little magmatic overprinting.

To the south, recent propagation of the VFR produced a very narrow zone of abyssal hill fabric. Seamounts and arcuate ridges adjacent to abyssal hill fabric, but within the broad and irregular Brunhes Chron support a history of diffuse crustal accretion for both off-axis terrain and terrain beyond the southern extent of spreading.

4.5 Northern Basin

Little can be interpreted from the modest amount of data in the northern basin beyond that of previous studies. It is apparent that spreading in this region is partitioned across multiple axes, but there are no GPS stations and few distinct plate boundaries to aid in defining plate motions within the basin; GPS data constrain only the total opening rates across the northern basin (Niuatoputapu to Lau Ridge stations [*Bevis et al.*, 1995]). The broad, shallow platform in the northeast Lau Basin, however, is largely encircled by distinct plate boundaries including the FRSC and NELSC to the west and the Tonga Trench to the north and east. This terrain has been interpreted as a part of the Tonga Plate, but geodetic analysis has demonstrated that its motion has a slight northward component in relation to other GPS stations within the Tonga Plate the to the south. This terrain may, in fact, be an independent Niuatoputapu microplate. West of the FRSC there is a well-defined morphologic boundary between the platform and the basin floor. This boundary may have represented the eastern extent of seafloor spreading before the FRSC propagated into the platform. With seafloor much shallower than that of the basin floor, it is unlikely that this crust formed via seafloor spreading, and instead may have existed as part of the Lau-Tonga Arc Complex before rifting began, or it may be the arc platform of the Tofua Arc in this region. In depth analysis of the character of this terrain is hindered by a lack of data beyond predicted bathymetry from satellite altimetry. Along the FRSC, most of the lavas sampled have an arc signature and the adjacent section of the Tofua Arc is inactive, indicating that at very close arc proximity, all arc magmatism can be captured by the backarc spreading center [*Keller et al.*, 2008].

4.6 Tofua arc

As mentioned above, asymmetry of central basin fabric and magnetic anomalies indicates the Tofua Arc may be built upon crust formed by seafloor spreading, though abyssal hill fabric and magnetic lineations are not apparent. Interpreting the pseudofault and the sharp western margin of the Tonga Ridge as conjugates indicates that all of this terrain formed when the central basin began opening. However, it is possible that the Tofua Arc and the western basin proto-arc formed as one feature during western basin opening, and ELSC propagation led to some intra-arc rifting, leaving only a small portion of the arc in the western basin. Western basin volcanic edifices may have been part of the early Tofua Arc before ELSC propagation stranded them within the western basin. South of 18º40 S, there is no morphologic boundary between the arc platform and the basin floor. Infill by eroded sediments from the Tonga Ridge in addition to volcaniclastic sediments from the arc has covered any older distinguishable seafloor morphology surrounding the arc volcanoes. Furthermore, lava flows from the arc volcanoes have magnetic signatures contrasting with this crust, creating an irregular magnetization pattern.

4.7 Tonga Ridge

The basin-side margins of the Tonga Ridge and Lau Ridge are very dissimilar, suggesting they are not direct conjugates. Following the opening of the western basin via multiple processes, the majority of the central basin crust (~17ºS to 21ºS) formed through seafloor spreading, creating the pseudofault and possibly influencing the formation of the

sharp western margin of the Tonga Ridge. Conversely, the differing structural natures of the original ridges may have led to this discrepancy. The Tonga Ridge was the forearc platform; possibly a stronger block of lithosphere supported by the subducting slab, and the Lau Ridge was the active arc, which was inherently more heterogeneous and had continuing volcanism during basin opening. The Tonga Ridge may have rifted more cleanly, while the Lau Ridge may have been altered by volcanism after rifting. Further complicating the history of the Tonga Ridge is the GPS evidence that deformation may be occurring within the Tonga Plate [*Phillips*, 2003]. The changing character of the Tonga Ridge from the south to the north and the transition to a broad platform north of 18º30'S suggests that the locus of rifting may have transitioned from more arc-ward to the south, where the ridge is wider to trench-ward to the north, where the ridge becomes narrower, though these variations may have been inherent in the original Lau-Tonga Ridge complex.

4.8 Basin Kinematics

Several effects may lead to non-rigid plate kinematics in the Lau Basin. Because extension is driven by trench roll back, changes in the shape of the trench may be accommodated by deformation of previously accreted crust. The Australia-Tonga pole is considered accurate for at least the duration of the Brunhes [*Zellmer and Taylor*, 2001], and most anomalies in the western basin are oriented subparallel to radial lines from the pole, indicating it may be accurate for the entirety of basin opening. The north and south extent of this consistency, however, is limited to the length of the modern ELSC.
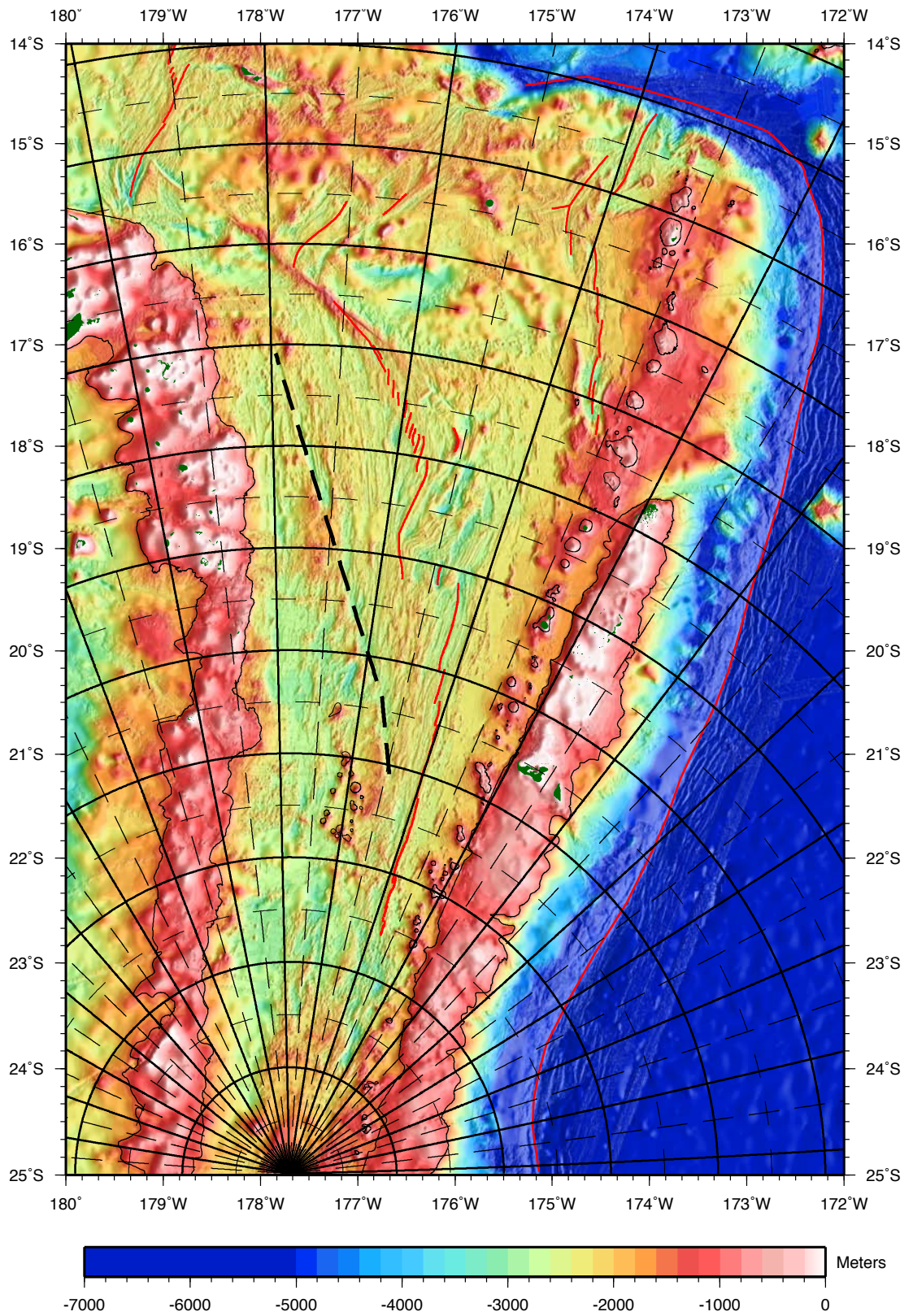
Figure 4.3. Bathymetry overlain by flow lines and radial lines of the Australia
Tonga pole [*Zellmer and Taylor*, 2001]. Flow lines are in 1-degree (solid) and 0.5-

degree (dashed) increments, and radial lines are in 10-degree (solid) and 5-degree (dashed) increments. Other symbols are as in Figure 1.3. Radial lines and flow lines demonstrate the variable orientation of abyssal fabric formed throughout basin opening, indicating that the Australia-Tonga pole may have migrated.

One model suggests that subduction of the Louisville Ridge has acted as a southward migrating "lock" on basin opening, necessitating deformation of the Tonga Plate and a migrating Australia-Tonga pole [*Ruellan et al.*, 2003]. Additionally, seismicity, GPS studies and the distribution of basin opening across multiple spreading centers suggest that numerous microplates exist in the northern basin [*Conder and Wiens*, 2011; *Ekström*, 2011; *Phillips*, 2003], many with unidentified and possibly diffuse boundaries. For example, the Niuafoʻou Microplate is only partially encircled by distinct boundaries; leading to the proposal of broad, diffuse plate boundaries without well-defined locations [*Zellmer and Taylor*, 2001]. A basin reconstruction using rigid plate kinematics is hindered by these factors.

While abyssal hill fabric within the central basin intersects the pseudofault, its orientation with respect to the Tonga ridge is unclear, due in part to heavy sedimentation adjacent to the ridge. North of 22º30'S, the sharp western margin is subparallel to radial lines from the Australia-Tonga opening pole, as well as being subparallel to abyssal hill fabric along the axis. A propagating margin such as a pseudofault, however, would likely show evidence of its formation with progressively younger crust intersecting it in the direction of propagation. The sharp western margin of the Tonga Ridge shows no such progression, but overprinting from the arc volcanoes obscures any contact between abyssal hill fabric and the Tonga Ridge. Non-rigid plate tectonics may have occurred

within the Tonga plate, proximal to the locus of a migrating Australia-Tonga Pole, while the Australian Plate has trailed passively and remained rigid.

The diffuse southern boundary of the Niuafoʻou Microplate (with the Tonga Plate) has been interpreted as connecting the southern tip of FRSC to the southern tip of the CLSC [*Zellmer and Taylor*, 2001], resulting in the CLSC and LETZ forming a boundary between the Australian Plate and the Niuafoʻou Microplate. However, this southern boundary is not well defined, as there is little seismic or morphologic data that illuminates its width and character. Additionally, there are limited locations where Brunhes-Matuyama boundary pairs can aid in constraining plate motion across the CLSC, as it has propagated southward during the Brunhes. Some recent (Brunhes-era) crustal formation in this region occurred along now extinct sections of the ELSC that were replaced by the propagating CLSC. Because this crust is transferred lithosphere, potentially young, positively magnetized crust is found apart from any currently active spreading centers—separate from the positively magnetized crust surrounding the CLSC and LETZ. This separation and further deformation degrades or invalidates the magnetization inversion in this region, impeding precise estimation of the width of the Brunhes anomaly along the CLSC.

The distributed deformation predicted for the southern boundary of the Niuafoʻou Microplate depends on how much of the total Brunhes width cannot be explained by the Tonga-Australia opening pole. However, measurements of the total Brunhes width across the CLSC and failed segments of the ELSC produce inconsistent results (*Figure 4.5*). In places, estimates of the total Brunhes width measured along Tonga-Australia flow lines

(to attempt to constrain the location of the Tonga-Australia-Niuafoʻou triple junction) meet the required width, yet in other places they do not.
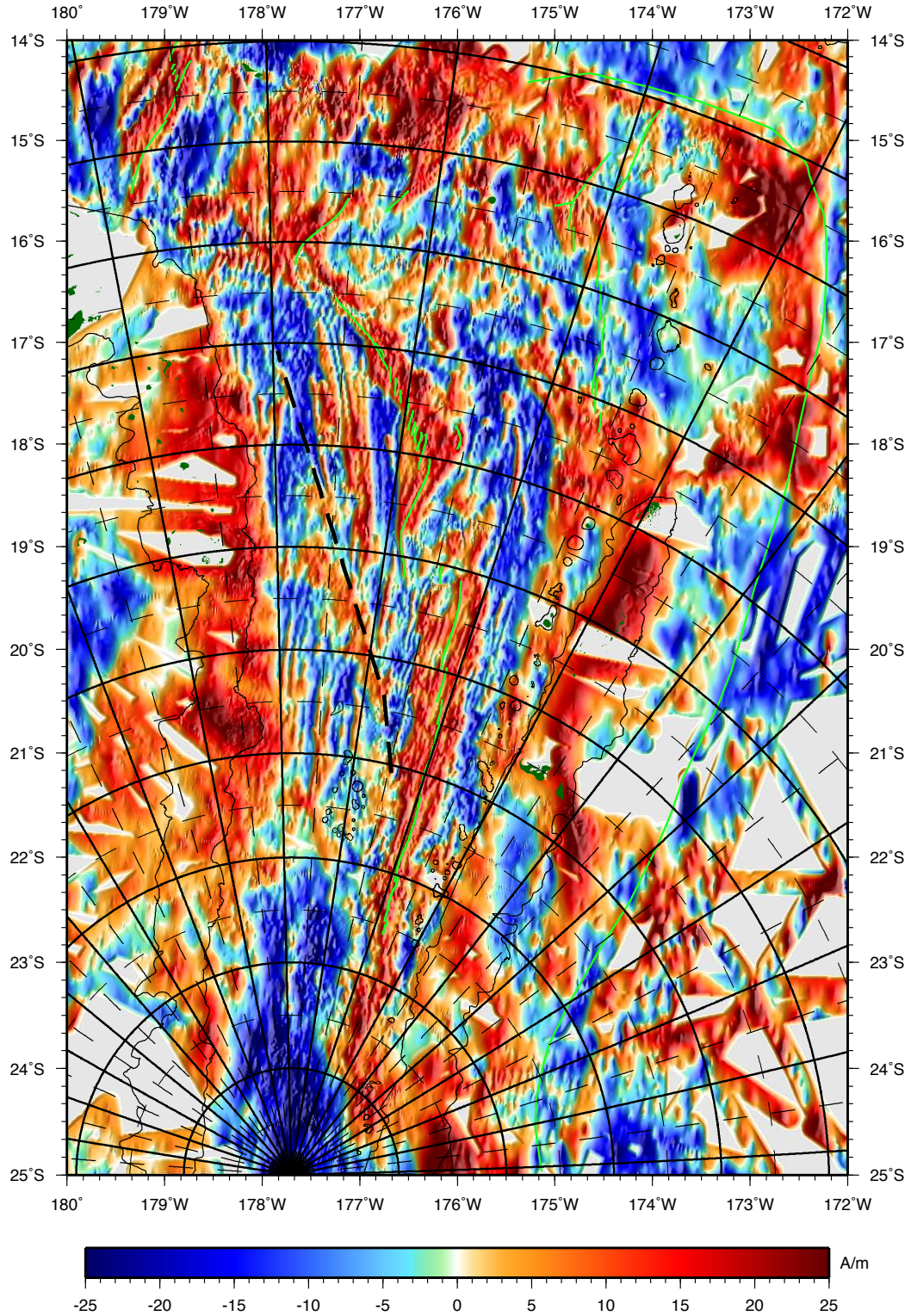
Figure 4.4. Magnetization overlain by flow lines and radial lines of the Australia-Tonga pole. Flow lines and radial lines are as in Figure 4.3. Light green lines indicate plate boundaries, and other symbols are as in Figure 1.3.

The irregular width of the Brunhes in this area may be explained by crustal rotations associated with the overlap zone between the CLSC and northern ELSC segments. Such crustal rotations would violate the assumptions of the magnetization inversion and possibly produce distorted magnetization polarity geometries. Another possible explanation may be continued volcanic emplacements in this area associated with the tectonic deformation of the overlap zone rather than Tonga-Australia extensional opening. Because of the structural complexity of this area we cannot refine the precise boundary of the predicted Niuafo'ou Microplate from the analysis of Zellmer and Taylor [2001].
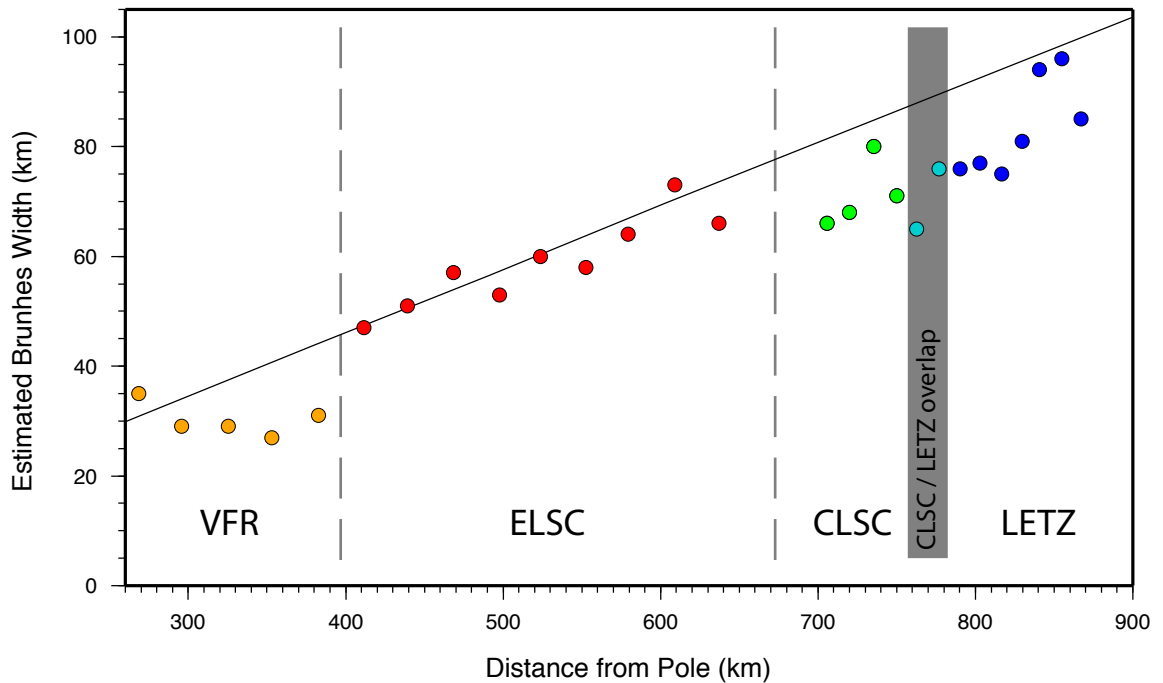
Figure 4.5. Estimated Brunhes anomaly width plot. Expected (line) vs. actual (points) based on the Australia-Tonga pole and an opening rate of 8.4°/Myr

68

[*Zellmer and Taylor*, 2001], and distances along flow lines. Dashed lines indicate transitions between spreading centers, and the CLSC and LETZ overlap is highlighted in gray. It is not clear which plate boundary (Australia-Tonga vs. Australia-Niuafoʻou) the CLSC and LETZ represent, and apparent deformation degrades the magnetization inversion east of the CLSC. The VFR has propagated during the Brunhes, so the Brunhes anomaly along it is not full width.

5. Conclusions

We conclude that the Lau Basin underwent a complex early opening history primarily characterized by various forms of magmatic crustal accretion instead of a protracted phase of tectonic rifting of pre-existing arc crust. Evolution of the western basin included organized seafloor spreading, diffuse magmatic crustal accretion, and possibly the development of a proto-arc, after a brief phase of rifting. As arc magmatism migrated eastward with the opening of the western basin, a new phase of organized spreading initiated in the northern central basin and propagated southward, ending extension and magmatic activity in the western basin. A pseudofault thus forms the boundary between the new central basin and western basin. The central basin has undergone a complicated morphologic evolution as well, as plate motions have reorganized and southward propagation continues. Furthermore, possible pole migration and changes to the shape of the trench during rollback have necessitated deformation from non-rigid opening within the basin. Along active spreading centers, variable magmatism has created abrupt changes in crustal structure. South of the organized spreading centers, diffuse terrain is found, which may have proxies in other parts of the basin. Mantle processes that vary with proximity to subduction, including chemical variations such as water, may control these fluctuations in modes of crustal accretion.

0 Ma

Lau Ridge   Lau Basin   Tofua   Tonga   Tonga
                                        Arc   Ridge   Trench

19°45 S, 179°30 W

Remnant Arc *Rifted Arc* *Remnant Axis* *Remnant Proto-Arc* *Pseudofault* *Active Axis* *Active Arc* *Remnant Forearc* *Trench*

22°15 S, 172°30 W

Western Basin   Central Basin

Australian Plate   **Tonga Plate**   **Pacific Plate**

km 0   100   200   300   400   500   600   700

1.5~1.7 Ma

Lau Ridge   Lau Basin   Tonga   Tonga
                              Ridge   Trench

Remnant Arc *Rifted Arc* *Active Axis* *Active Arc* *Remnant Forearc* *Trench*

Western Basin

Australian Plate   **Tonga Plate**   **Pacific Plate**

km 0   100   200   300   400   500   600

6 Ma

Lau-Tonga Ridge   Tonga Trench

Arc   *Forearc*   *Trench*

Australian Plate   **Pacific Plate**

km 0   100   200   300   400

71

Figure 5.1. Bathymetric cross section showing stages of Lau Basin evolution over 6 Ma at 9x vertical exaggeration. Crustal thickness is estimated isostatically from bathymetry, except where the forearc is supported by the subducting plate [*Martinez and Taylor*, 2002]. At 0 Ma, the cross section is of the basin in its current state. At 1.5-1.7 Ma, the central basin is closed (along this transect) leaving the western basin, and at 6 Ma the basin is closed entirely, leaving the original Lau-Tonga Ridge complex.

5.1 Importance

Processes in backarc basins are broadly relevant in plate tectonics, in part, due to their similarity to mid-ocean ridge processes, which have produced the vast majority of Earth's crust. However, in backarc basins, effects of variable mantle chemistry due to subduction can be strongly expressed in arc-proximal ridges and show systematic variations with distance from the trench and can thus serve to demonstrate the effects of variable mantle chemistry on seafloor spreading characteristics in general. They also have implications for exploration of minerals (including copper, gold, zinc, and silver) as well as for understanding the character of subduction. Studying the thermal, rheological, and especially chemical factors within backarc basins aids in constraining the variations of oceanic crustal accretion and how they relate to arc-proximity. However, the controls on plate boundaries appear to fall along a continuum from mid-ocean ridge-like and narrow to strongly subduction-influenced and diffuse, leading to somewhat ambiguous behavior, and a range of seismic structures. The more silicic and volatile-rich environment (with respect to mid-ocean ridge settings) may also be a proxy to the early Earth, before volatiles decreased in concentration due to extraction into the continental crust.

5.2 Future Work

A whole-basin plate tectonic reconstruction was hindered by a lack of data, particularly in off-axis regions, as well as north and south of the focus of this study. More thorough geophysical mapping surveys, particularly to the north and south, would help determine systematic changes throughout the basin. Furthermore, methodical sampling of off-axis lavas may help constrain the processes that led to the morphologic variations identified in this paper. This would be especially beneficial for a more complete understanding of the western basin, including seamounts, "ridges and knolls" terrain, and high backscatter patches, as well as determining whether the western basin platform is a young relict arc platform, older rifted arc terrain, or arc-like terrain. Additional seismic experiments could reveal crustal structures in heavily sedimented areas, including areas to the south that represent the early opening stage of the basin. Long term monitoring of small-scale seismic activity (via a seismic array or hydrophones) would support more comprehensive identification of plate boundaries. Lastly, GPS stations in the northern basin (e.g. around Niuafoʻou) could constrain microplate motions.

Appendix

Introduction

Data collected throughout 2009 on R/V Langseth, R/V Onnuri, and R/V Revelle cruises in the western Lau Basin show lineated seafloor features that were not detected in previous low-resolution studies. Track spacing of 5 arc minutes exposes areas of apparent abyssal seafloor fabric that are disrupted by more hummocky terrain, possible arc-type volcanism and transferred lithosphere containing broad magnetization patterns. The lineated, short-wavelength, discontinuous magnetic lineations behave in manners somewhat inconsistent with seafloor magnetization processes. Inversion of total field anomaly data to solve for seafloor magnetization produces anomalies that seem to disappear at points, but actually continue below 0 A/m. Additionally, large irregular areas of crust appearing to be negatively magnetized are contained within the positive Brunhes Chron, adjacent to the active spreading centers.

Assumptions in the inversion process may contribute to the anomalous features observed. As a positive magnetic field dominates the relatively young opening history of the basin, an inversion that balances positive and negative anomalies is likely to be inaccurate. Furthermore, while the inversion supposes a constant source layer thickness, variations in magmatic production (due to arc proximity) could potentially cause the source layer thickness to be non-uniform. This may lead to irregular variations in strength and polarity. Addition of a magnetic annihilator creates a more accurate solution to the inversion calculation.
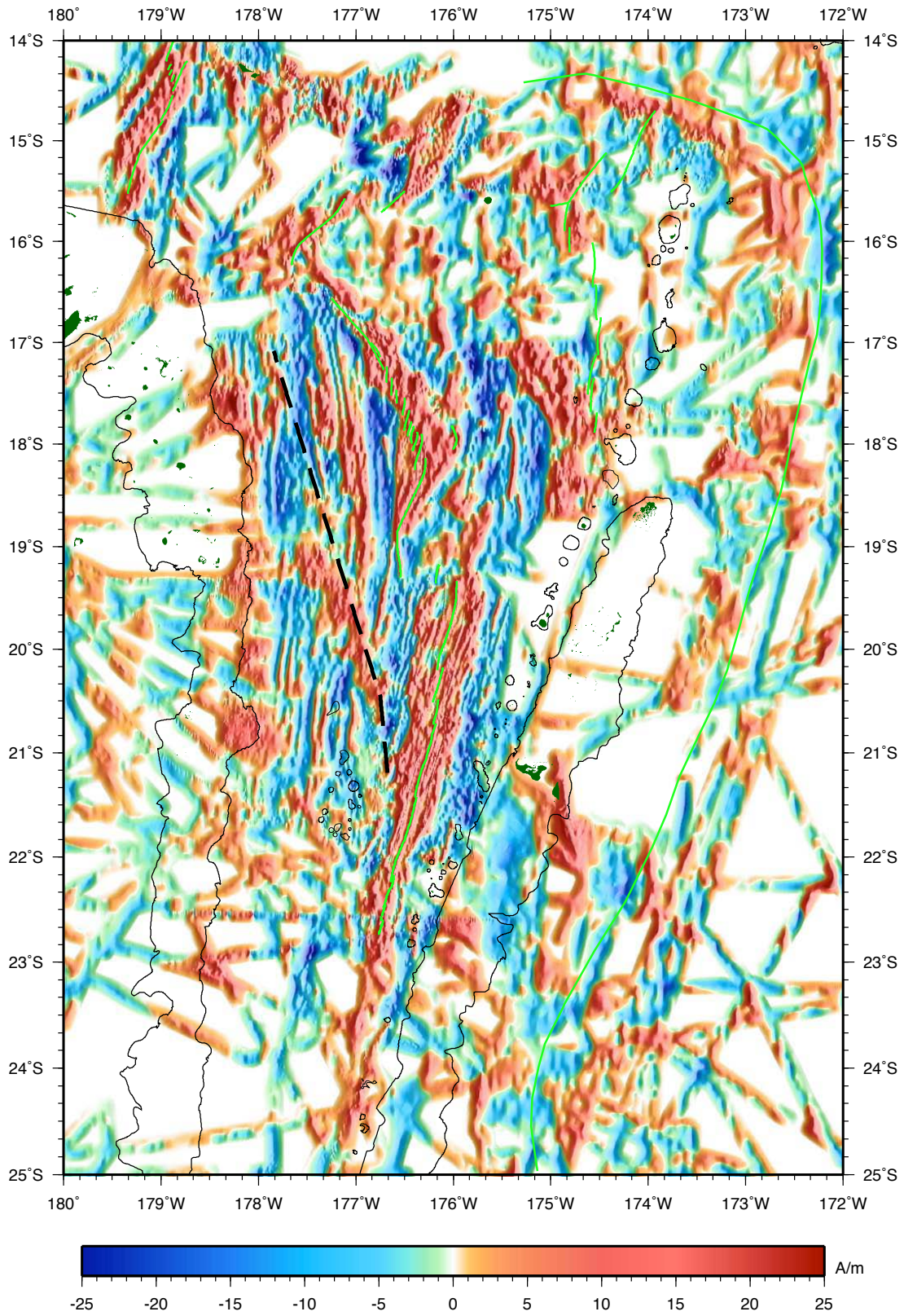
Figure A1. Estimated seafloor magnetization of the Lau Basin without annihilator. Bathymetry was reduced to 0.5-arc-minute resolution and points shallower than

500 m were clipped to 500 m for the inversion, which assumed a 0.5-km source layer. Light green lines indicate plate boundaries, the pseudofault is represented by a dashed black line, and subaerial features are in dark green. Tofua Arc volcanoes are outlined with 800-m contours, while other features are outlined with simplified 1,450-m contours. *Note: annihilator tests were performed with a previous data compilation.*

Methods

A magnetic annihilator is a distribution of magnetization that creates no magnetic field. A given area of magnetized seafloor can be composed of both an annihilator part as well as a non-annihilator part. Therefore, solving for magnetization by inverting a magnetic field is a non-unique problem. Following inversion, any amount of an annihilator can be added to or subtracted from a magnetization to create the same magnetic field.

From the equation for the total field anomaly following Parker and Huestis [1974] and Blakely [1996]:

$$\mathcal{F}[\Delta T] = 2\pi C_m \Theta_m \Theta_f e^{|k|z_0} \left(1 - e^{-|k|t}\right) \sum_{n=0}^{\infty} \frac{\left(-|k|\right)^n}{n!} \mathcal{F}[M z_1^{\ n}]$$

For $k = 0$, $1 - e^{-|k|t} = 0$, so any distribution of magnetization (M), will create zero total field anomaly (ΔT).

By setting a delta function equal to a magnetization distribution (a),

$$\delta(k_x)\delta(k_y) = \sum_{n=0}^{\infty} \frac{\left(-|k|\right)^n}{n!} \mathcal{F}[a z_1^{\ n}]$$

power is removed from everything except the zero wavenumber; $\delta(k_x) = 0$ and $\delta(k_y) = 0$ for anything other than $k_x, k_y = 0$.

For $n = 0$, $\dfrac{\left(-|k|\right)^n}{n!}\mathcal{F}\left[Mz_1{}^n\right]$ is reduced to $\mathcal{F}[M]$. Using this, we can separate out

the $n = 0$ term, and substitute (a) for (M):

$$\delta\left(k_x\right)\delta\left(k_y\right) = \mathcal{F}[a] + \sum_{n=1}^{\infty}\frac{\left(-|k|\right)^n}{n!}\mathcal{F}\left[az_1{}^n\right]$$

rearranging to get:

$$\mathcal{F}[a] = \delta\left(k_x\right)\delta\left(k_y\right) - \sum_{n=1}^{\infty}\frac{\left(-|k|\right)^n}{n!}\mathcal{F}\left[az_1{}^n\right]$$

an equation for a magnetic annihilator. This is solved iteratively, by estimating the

magnetization on the right, solving the equation, updating the initial estimate and

repeating the process until the solution converges.

Another method for calculating an annihilator is presented in Tivey's MATLAB

code *ann3d.m* [2010], based on the Fortran77 code of Macdonald et al. [1980]. For a

given bathymetric distribution, a uniform magnetization distribution is created and the

two are forward modeled to solve for the total field anomaly. This magnetic field is then

inverted with the bathymetry to find a second magnetization distribution that would

create an identical field. As both distributions create the same field, the difference

between the two creates no field, and is therefore a magnetic annihilator.

Again, starting from the equation for a total field anomaly, for a given

magnetization, (M):

$$\mathcal{F}[\Delta T] = 2\pi C_m \Theta_m \Theta_f e^{|k|z_0}\left(1 - e^{-|k|t}\right)\sum_{n=0}^{\infty}\frac{\left(-|k|\right)^n}{n!}\mathcal{F}\left[M z_1{}^n\right]$$

we can derive the inverse equation by first separating out the $n = 0$ term, $\mathcal{F}[M]$

$$\mathcal{F}[\Delta T] = 2\pi C_m \Theta_m \Theta_f e^{|k|z_0} \left(1 - e^{-|k|t}\right) \left[\mathcal{F}[M] + \sum_{n=1}^{\infty} \frac{(-|k|)^n}{n!} \mathcal{F}[M z_1^{\;n}] \right]$$

and rearranging to get:

$$\mathcal{F}[M] = \frac{\mathcal{F}[\Delta T]}{2\pi C_m \Theta_m \Theta_f e^{|k|z_0} \left(1 - e^{-|k|t}\right)} - \sum_{n=1}^{\infty} \frac{(-|k|)^n}{n!} \mathcal{F}[M z_1^{\;n}]$$

Assigning the original magnetization to (M_1), the second to (M_2), and substituting the forward equation into the inverse equation, we get:

$$\mathcal{F}[M_2] = \frac{2\pi C_m \Theta_m \Theta_f e^{|k|z_0} \left(1 - e^{-|k|t}\right) \sum_{n=0}^{\infty} \frac{(-|k|)^n}{n!} \mathcal{F}[M_1 z_1^{\;n}]}{2\pi C_m \Theta_m \Theta_f e^{|k|z_0} \left(1 - e^{-|k|t}\right)} - \sum_{n=1}^{\infty} \frac{(-|k|)^n}{n!} \mathcal{F}[M_2 z_1^{\;n}]$$

simplifying to:

$$\mathcal{F}[M_2] = \sum_{n=0}^{\infty} \frac{(-|k|)^n}{n!} \mathcal{F}[M_1 z_1^{\;n}] - \sum_{n=1}^{\infty} \frac{(-|k|)^n}{n!} \mathcal{F}[M_2 z_1^{\;n}]$$

We then take the difference between (M_1) and (M_2),

$$\mathcal{F}[M_2 - M_1] = \mathcal{F}[M_2] - \mathcal{F}[M_1]$$

and substitute in the equation for (M_2):

$$\mathcal{F}[M_2 - M_1] = \sum_{n=0}^{\infty} \frac{(-|k|)^n}{n!} \mathcal{F}[M_1 z_1^{\;n}] - \sum_{n=1}^{\infty} \frac{(-|k|)^n}{n!} \mathcal{F}[M_2 z_1^{\;n}] - \mathcal{F}[M_1]$$

We can then separate the $n = 0$ term ($\mathcal{F}[M_1]$) out of the first summation:

$$\mathcal{F}[M_2 - M_1] = \mathcal{F}[M_1] + \sum_{n=1}^{\infty} \frac{(-|k|)^n}{n!} \mathcal{F}[M_1 z_1^{\;n}] - \sum_{n=1}^{\infty} \frac{(-|k|)^n}{n!} \mathcal{F}[M_2 z_1^{\;n}] - \mathcal{F}[M_1]$$

simplifying to:

$$\mathcal{F}[M_2 - M_1] = \sum_{n=1}^{\infty} \frac{(-|k|)^n}{n!} \mathcal{F}[(M_1 - M_2) z_1^{\;n}]$$

rearranging to:

$$\mathcal{F}[M_2 - M_1] = -\sum_{n=1}^{\infty} \frac{\left(-|k|\right)^n}{n!} \mathcal{F}\left[(M_2 - M_1)z_1^{\,n}\right]$$

Rewriting $(M_2 - M_1)$ as (a) we get:

$$\mathcal{F}[a] = -\sum_{n=1}^{\infty} \frac{\left(-|k|\right)^n}{n!} \mathcal{F}\left[az_1^{\,n}\right]$$

rearranging to:

$$\mathcal{F}[a] + \sum_{n=1}^{\infty} \frac{\left(-|k|\right)^n}{n!} \mathcal{F}\left[az_1^{\,n}\right] = 0$$

The $n = 0$ term ($\mathcal{F}[a]$) can be added back in:

$$\sum_{n=0}^{\infty} \frac{\left(-|k|\right)^n}{n!} \mathcal{F}\left[az_1^{\,n}\right] = 0$$

Substituting back into the total field anomaly equation:

$$\mathcal{F}[\Delta T] = 2\pi C_m \Theta_m \Theta_f e^{|k|z_0}\left(1 - e^{-|k|t}\right)\sum_{n=0}^{\infty} \frac{\left(-|k|\right)^n}{n!} \mathcal{F}\left[az_1^{\,n}\right] = 0$$

This distribution of magnetization creates no field.

Using the software package Mirone, a graphical user interface for manipulating GMT grids, an initial inversion was performed resulting in the magnetization map in *Figure A1* [*Luis*, 2007]. Mirone was further used to calculate an annihilator, according to the Macdonald method above.

Starting uniform magnetization grids of 1.0, 2.5, 5.0 and 10.0 A/m were used for the initial forward calculations. Power is removed from the zero wavenumber to prevent 'blowups'. This insures that the inversion process will not return a grid of uniform magnetization; therefore the second magnetization grid will be different from the first.

The mean of the total field anomaly data is removed to normalize it before inverting for magnetization. Additionally, band-pass filtering is performed on the data

during the inversion process. Annihilator estimates were created both with and without these features. Finally, annihilator grids were forward calculated to verify that the magnetic fields they create are insignificant.

Results and Discussion

Annihilator grids retained an average magnetization equal to the original uniform magnetizations and will be referred to by these numbers (1.0, 2.5, 5.0 and 10.0 A/m). They all produce magnetic fields averaging zero with standard deviation of 5.0 nT or less. In comparison, the total field anomaly range is generally ±500 nT throughout the basin with the amplitude of most anomalies exceeding 200 nT. All medians are 0.01 nT or less, indicating their variation from the mean is insignificant. Standard deviation and median both increase proportionally with the magnitude of the original uniform magnetization.

While there is effectively no difference between normalizing the magnetic field before inversion and not doing so, there is a very slight decrease in the magnitude of both standard deviation (<0.01 nT) and median (<0.001 nT) when no band-pass filtering is done. Removal of short wavelengths through band-pass filtering likely impedes the inversion's ability to account for sharp bathymetric changes.

Negative areas along axis within the Brunhes Chron are reduced slightly with the 1.0 nT annihilator added to the initial magnetization grid (*Figure A2*). These are further reduced with increasing annihilator magnitudes, but magnetic depressions can still be noted with the 10.0 nT annihilator added (*Figure A5*). These are generally near propagating ridge tips indicating that "trapped" negative crust or rotated positive crust may explain some portion of these features.

80
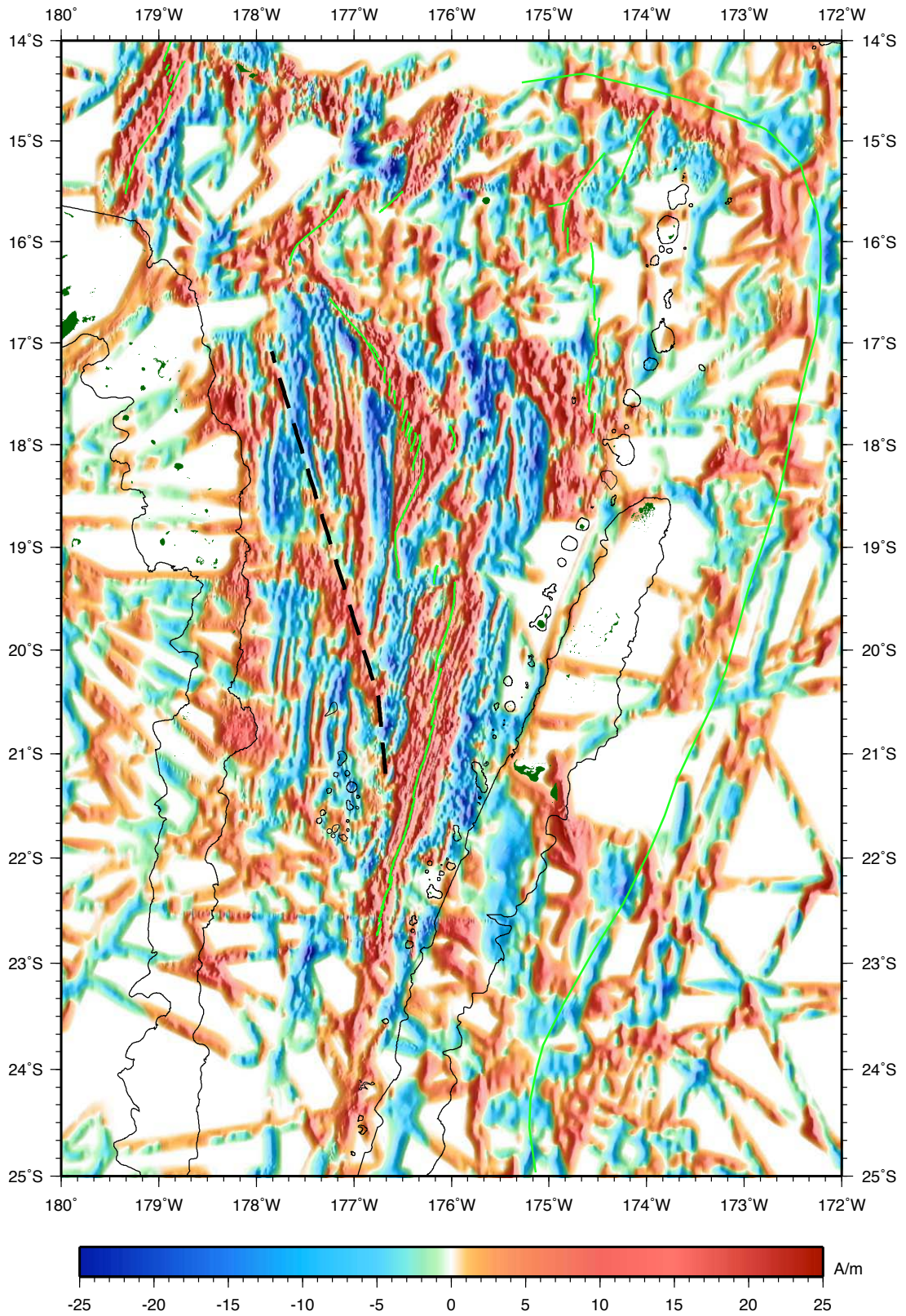
Figure A2. Estimated seafloor magnetization of the Lau Basin with an annihilator averaging 1.0 A/m added. Symbols are as in Figure A1.
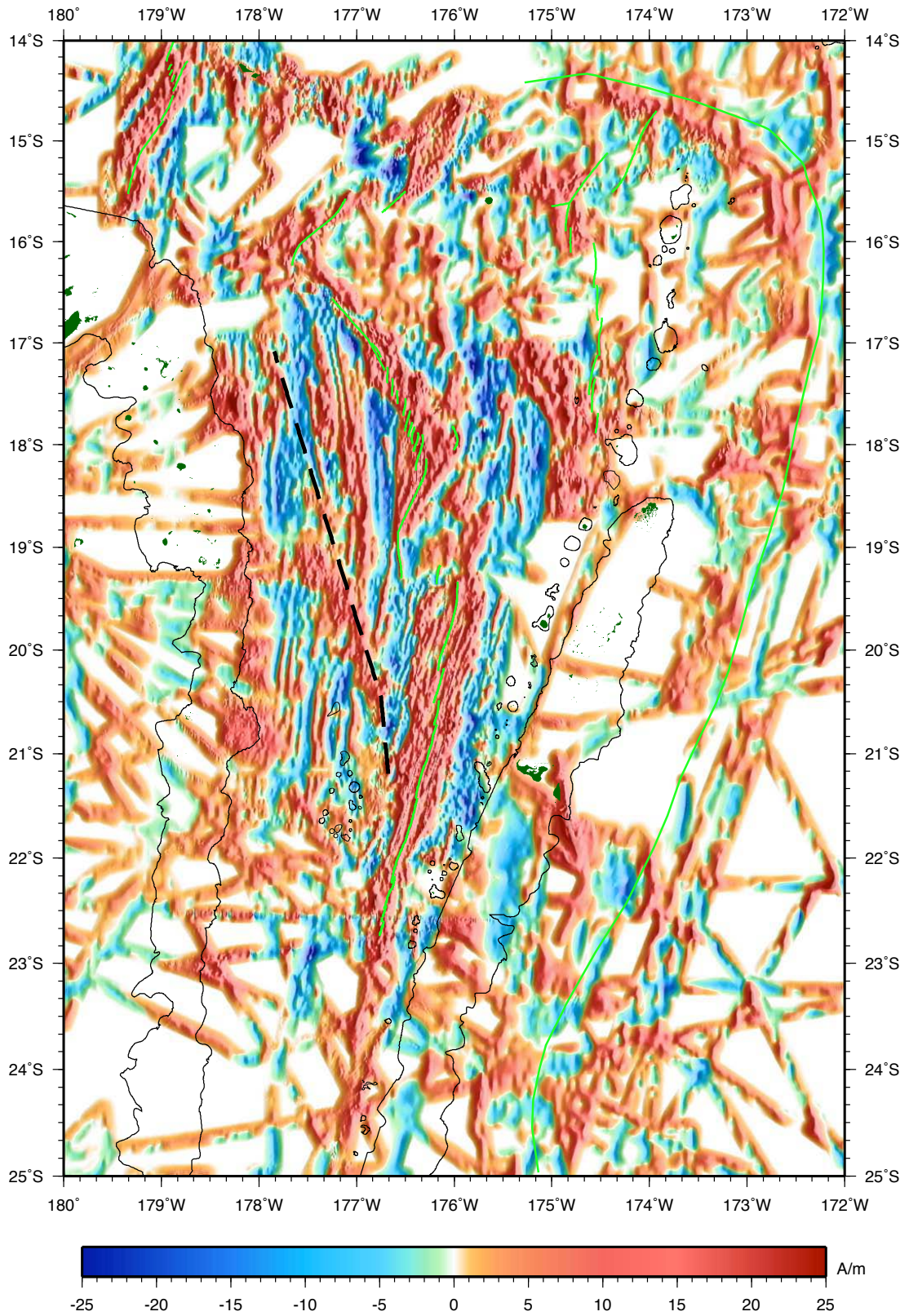
Figure A3. Estimated seafloor magnetization of the Lau Basin with an annihilator averaging 2.5 A/m added. Symbols are as in Figure A1.
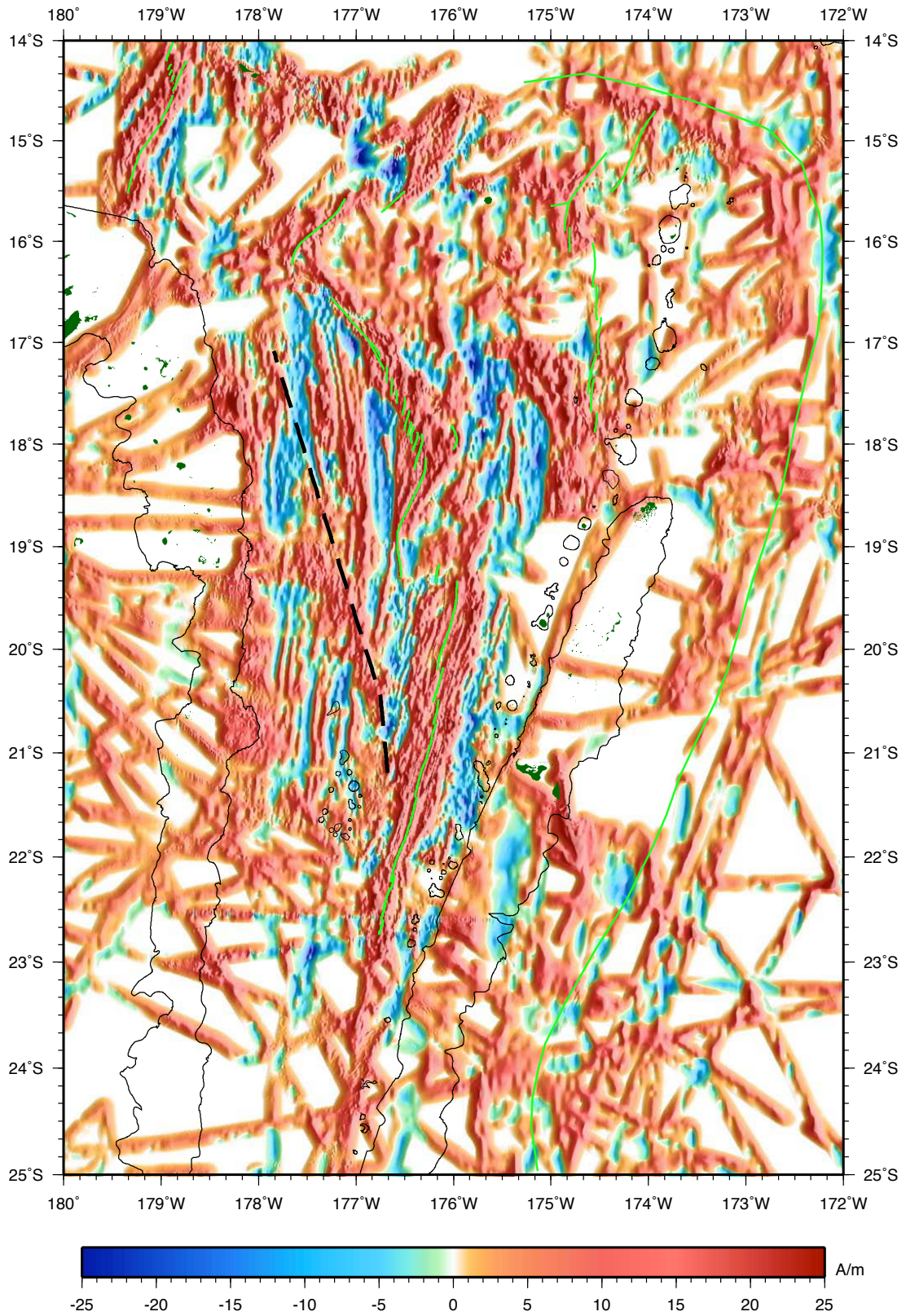
Figure A4. Estimated seafloor magnetization of the Lau Basin with an annihilator averaging 5.0 A/m added. Symbols are as in Figure A1.
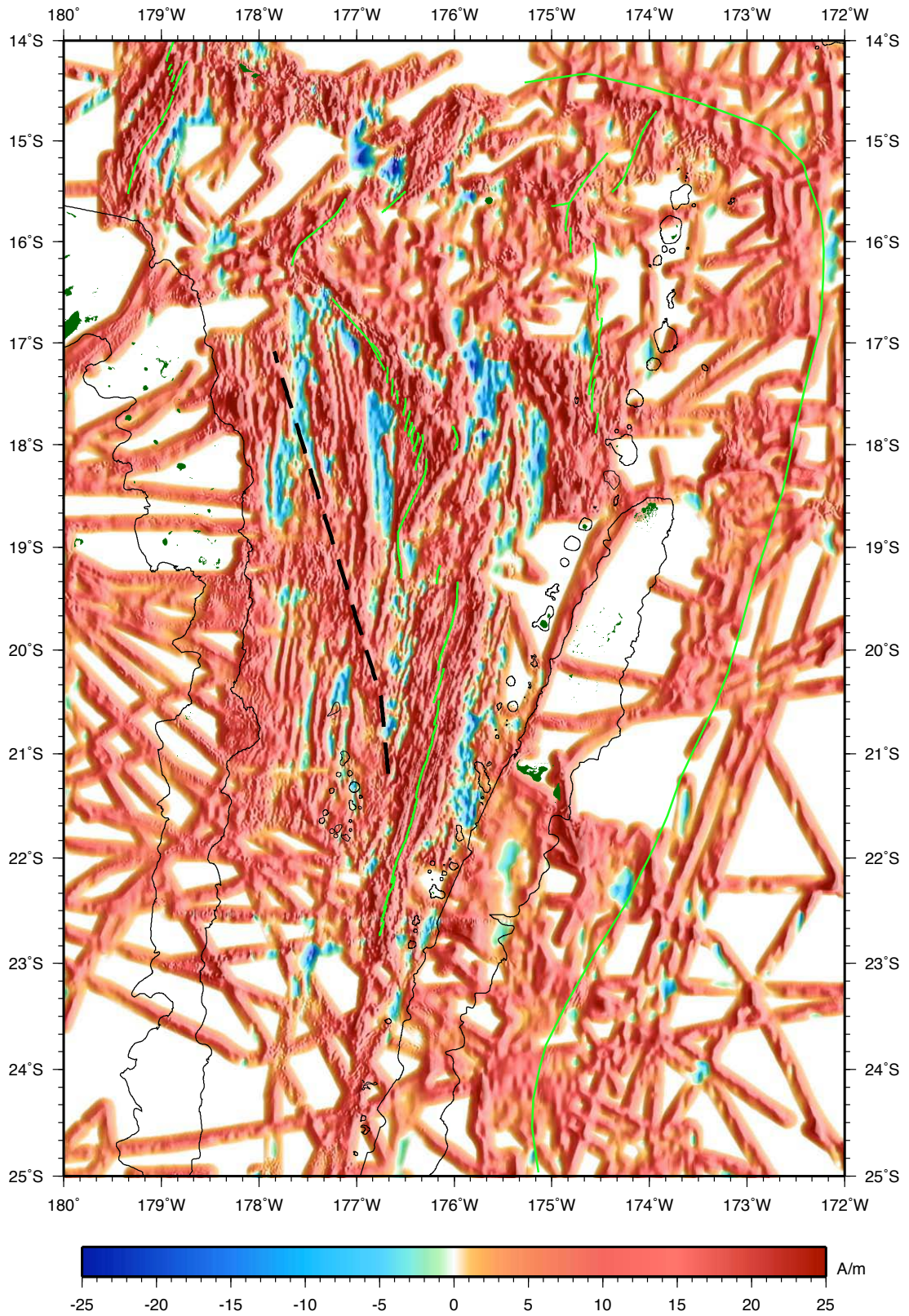
Figure A5. Estimated seafloor magnetization of the Lau Basin with an annihilator averaging 10.0 A/m added. Symbols are as in Figure A1.

The boundaries of the Brunhes Chron remain the same despite the addition of a magnetic annihilator until the 10.0 nT annihilator, which causes many anomalies to blend together. Lineations in the western basin, which are not consistently positive, but are shown as continuous when the anomalies are illuminated show some improvement but do not become fully positive until the 5.0 nT annihilator is added (*Figure A4*). Despite the addition, some anomalies further to the north still appear to 'turn negative'. The Lau Ridge, mapped in parts by numerous survey boats entering or leaving the basin, shows the most dramatic difference between the 2.5 nT annihilator addition (*Figure A3*) and the 5.0 annihilator addition. The magnetization, which initially appears positive on both edges of the ridge, but negative in the center, becomes almost consistently positive with the 5.0 nT annihilator. The magnetization pattern is similar to the field that would be created by a uniformly magnetized ridge, but the inversion process should account for edge effects.

Conclusion

Following the magnetic inversion method of Parker and Huestis [1974], and Macdonald et al. [1980] a magnetization distribution that effectively creates no magnetic field can be calculated to fit a given bathymetry distribution. However, hinderances in an inversion such as sediment infill (which can alter bathymetry) and rotation of crust can't be fully accounted for by the addition of an annihilator. Despite these issues, in the Lau Basin both 2.5 nT and 5.0 nT annihilators offer significant improvement to the magnetization map while 1.0 nT and 10.0 nT annihilators offer too little and too much respectively. The 2.5 nT annihilator improves the continuity of lineations in the western

85

basin, allowing for better correlation of the seafloor magnetization pattern with the

earth's magnetic field reversal time scale.

References Cited

Arculus, R. J. (2008), Structure, Evolution, Petrology and Hydrothermal Activity of Spreading Centres in the Northern Lau Backarc Basin, Marine National Facility Voyage Summary SS07/2008, http://www.cmar.csiro.au/datacentre/process/data_files/cruise_docs/SS200807sum.pdf, 23 pp.

Austermann, J., Z. Ben-Avraham, P. Bird, O. Heidbach, G. Schubert, and J. M. Stock (2011), Quantifying the forces needed for the rapid change of Pacific plate motion at 6 Ma, Earth Planet. Sci. Lett, 307, 289-297.

Bevis, M. (1997), Geodetic measurements in the Tonga-Lau arc system (abstract), Eos Trans. AGU, 78, 697-698.

Bevis, M., et al. (1995), Geodetic observations of very rapid convergence and back-arc extension at the Tonga arc, Nature, 374, 249-251.

Blakely, R. J. (1996), Potential Theory in Gravity and Magnetic Applications, 464 pp., Cambridge University Press, New York, NY.

Caress, D. W., and D. N. Chayes (2006), MB-System: Mapping the Seafloor, http://www.mbari.org/data/mbsystem and http://www.ldeo.columbia.edu/res/pi/MB-System.

Carlson, R. L., and P. J. Melia (1984), Subduction hinge migration, Tectonophysics, 102, 399-411.

Cherkis, N. Z. (1980), Aeromagnetic investigations and sea floor spreading history in the Lau Basin and northern Fiji Plateau, in Symposium on Petroleum Potential in Island Arcs, Small Ocean Basins, Submerged Margins, and Related Areas, edited by W. J. Clark, 37-45, New Zealand Dept. of Sci. and Ind. Res., Wellington.

Conder, J. A., and D. A. Wiens (2011), Shallow seismicity and tectonics of the central and northern Lau Basin, Earth Planet. Sci. Lett., 304, 538-546.

Conder, J. A., D. A. Wiens, and J. Morris (2002), On the decompression melting structure at volcanic arcs and back-arc spreading centers, Geophys. Res. Lett., 29(15), 1727, doi:1710.1029/2002GL015390.

Dunn, R. A., and F. Martinez (2011), Contrasting crustal production and rapid mantle transitions beneath back-arc ridges, Nature, 469, 198-202.

Ekström, G. (2011), The Global CMT Project, http://www.globalcmt.org/.

Ewart, A., and W. B. Bryan (1972), Petrography and Geochemistry of the Igneous Rocks from Eua, Tongan Islands, Geol. Soc. America Bull., 83(11), 3281-3298.

Fujiwara, T., T. Yamazaki, and M. Joshima (2001), Bathymetry and magnetic anomalies in the Havre Trough and southern Lau Basin: from rifting to spreading in back-arc basins, Earth Planet. Sci. Lett., 185, 253-264.

Gill, J. B. (1976), Composition and age of Lau Basin and Ridge volcanic rocks: Implications for evolution of an interarc basin and remnant arc, Geol. Soc. America Bull., 87(10), 1384-1395.

Hamburger, M. W., and B. L. Isacks (1988), Diffuse back-arc deformation in the southwestern Pacific, Nature, 332, 599-604.

Harmon, N., and D. K. Blackman (2010), Effects of plate boundary geometry and kinematics on mantle melting beneath the back-arc spreading centers along the Lau Basin, Earth Planet. Sci. Lett., 298, 334-346.

Hawkins, J. W. (1995), Evolution of the Lau Basin: Insights from ODP leg 135, in Active Margins and Marginal Basins of the Western Pacific, Geophys. Monogr. Ser., vol. 88, edited by B. Taylor and J. Natland, 125-173, AGU, Washington, D.C.

Hawkins, J. W., and J. T. Melchior (1985), Petrology of Mariana Trough and Lau Basin basalts, J. Geophys. Res., 90, 11431-11468.

Hawkins, J. W., and J. F. Allan (1994), Petrologic evolution of the Lau Basin sites 834 through 839, in Proc. ODP, Sci. Results, edited by J. Hawkins, L. Parson, J. Allan et al., 427-470, Ocean Drilling Program, College Station, TX.

Hawkins, J. W., L. Parson, J. Allen, et al. (1994), Proc. ODP, Sci. Results, 984 pp., Ocean Drilling Program, College Station, TX.

Hey, R. N. (1977), A new class of "pseudofaults" and their bearing on plate tectonics: a propagating rift model, Earth Planet. Sci. Lett, 37, 321-325.

Karig, D. E. (1970), Ridges and basins of the Tonga-Kermadec island arc system, J. Geophys. Res., 75, 239-254.

Katz, H. R. (1978), Composition and age of Lau Basin and Ridge volcanic rocks: Implications for evolution of an interarc basin and remnant arc: Discussion and reply, Geol. Soc. America Bull., 89(7), 1118-1120.

Keller, N. S., R. J. Arculus, J. Hermann, and S. Richards (2008), Submarine back-arc lava with arc signature: Fonualei Spreading Center, northeast Lau Basin, Tonga, J. Geophys. Res., 113, B08S07, doi: 10.1029/2007JB005451.

Kleinrock, M. C., and R. N. Hey (1989), Migrating transform zone and lithospheric transfer at the Galapagos 95.5°W propagator, J. Geophys. Res, 94, 13859-13878.

Langmuir, C. H. (2010), Personal Communication.

Lawver, L. A., and J. W. Hawkins (1978), Diffuse magnetic anomalies in marginal basins: their possible tectonic and petrologic significance, Tectonophysics, 45, 323-339.

Lawver, L. A., J. W. Hawkins, and J. G. Sclater (1976), Magnetic anomalies and crustal dilation in the Lau Basin, Earth Planet. Sci. Lett., 33, 27-35.

Luis, J. F. (2007), Mirone: A multi-purpose tool for exploring grid data, Computers & Geosciences, 33(1), 31-41.

Macdonald, K. C., S. P. Miller, S. P. Huestis, and F. N. Spiess (1980), Three-Dimensional modeling of a magnetic reversal boundary from inversion of Deep-Tow measurements, J. Geophys. Res., 85, 3670-3680.

Martinez, F., and B. Taylor (2002), Mantle wedge control on back-arc crustal accretion, Nature, 416, 417-420.

Martinez, F., and B. Taylor (2003), Controls on back-arc crustal accretion: insights from the Lau, Manus and Mariana basins, in Intra-Oceanic Subduction Systems: Tectonic and Magmatic Processes, Special Publications, vol. 219, edited by R. D. Larter and P. T. Leat, 19-54, Geological Society, London.

Martinez, F., and B. Taylor (2006), Modes of crustal accretion in back-arc basins: Inferences from the Lau Basin, in Back-Arc Spreading Systems: Geological, Biological, Chemical and Physical Interactions, Geophys. Monogr. Ser. vol. 166, edited by D. M. Christie, C. R. Fisher, S.-M. Lee and S. Givens, 5-30, AGU, Washington, DC.

Martinez, F., B. Taylor, E. T. Baker, J. A. Resing, and S. L. Walker (2006), Opposing trends in crustal thickness and spreading rate along the back-arc Eastern Lau Spreading Center: Implications for controls on ridge morphology, faulting, and hydrothermal activity, Earth Planet. Sci. Lett., 245, 655-672.

Maus, S., T. Sazonova, K. Hemant, J. D. Fairhead, and D. Ravat (2007), National Geophysical Data Center candidate for the World Digital Magnetic Anomaly Map, Geochem. Geophys. Geosyst., 8(6), Q06017, doi: 10.1029/2007GC001643.

Moberly, R. (1972), Origin of lithosphere behind island arcs, with reference to the western Pacific, in Studies in Earth and Space Sciences, A Memoir in Honor of Harry H. Hess, Memoir 132, edited by R. Shagam, R. B. Hargraves, W. J. Morgan, F. B. V. Houten, C. A. Burk, H. D. Holland and L. C. Hollister, 35-55, Geological Society of America, Boulder, Colorado.

Parker, R. L., and S. P. Huestis (1974), The inversion of magnetic anomalies in the presence of topography, J. Geophys. Res., 79, 1587-1593.

Parson, L. M., and J. W. Hawkins (1994), Two-stage ridge propagation and the geological history of the Lau backarc basin, in Proc. ODP, Sci. Results, edited by J. Hawkins, L. Parson, J. Allan et al., 819-828, Ocean Drilling Program, College Station, TX.

Parson, L. M., and I. C. Wright (1996), The Lau-Havre-Taupo back-arc basin: A southward-propagating, multi-stage evolution from rifting to spreading, Tectonophysics, 263, 1-22.

Parson, L. M., J. W. Hawkins, and P. M. Hunter (1992), Morphotectonics of the Lau Basin seafloor—implications for the opening history of back-arc basins, in Proc. ODP, Init. Repts., edited by L. Parson, J. Hawkins, J. Allan et al., 81-82, Ocean Drilling Program, College Station, TX.

Parson, L. M., R. G. Rothwell, and C. J. MacLeod (1994), Tectonics and sedimentation in the Lau Basin (southwest Pacific), in Proc. ODP, Sci. Results, edited by J. Hawkins, L. Parson, J. Allan et al., 9-21, Ocean Drilling Program, College Station, TX.

Parson, L. M., J. A. Pearce, B. J. Murton, and R. A. Hodkinson (1990), Role of ridge jumps and ridge propagation in the tectonic evolution of the Lau back-arc basin, southwest Pacific, Geology, 18, 470-473.

Pelletier, B., S. Calmant, and R. Pillet (1998), Current tectonics of the Tonga-New Hebrides region, Earth Planet. Sci. Lett., 164, 263-276.

Pelletier, B., Y. Lagabrielle, M. Benoit, G. Cabioch, S. Calmant, E. Garel, and C. Guivel (2001), Newly identified segments of the Pacific-Australia plate boundary along the North Fiji transform zone, Earth Planet. Sci. Lett, 193, 347-358.

Phillips, D. A. (2003), Crustal Motion Studies in the Southwest Pacific, Doctoral thesis, University of Hawaii at Manoa, Honolulu, HI.

Ruellan, E., J. Delteil, I. Wright, and T. Matsumoto (2003), From rifting to active spreading in the Lau Basin-Havre Trough backarc system (SW Pacific): Locking/unlocking induced by seamount chain subduction, Geochem. Geophys. Geosyst., 4(5), 8909, doi: 10.1029/2001GC000261.

Shipboard Scientific Party (1992), Introduction, background, and principal results of Leg 135, Lau Basin, in Proc. ODP, Init. Repts., edited by L. Parson, J. Hawkins, J. Allan et al., 5-47, Ocean Drilling Program, College Station, TX.

Smith, W. H. F., and D. T. Sandwell (1997), Global sea floor topography from satellite altimetry and ship depth soundings, Science, 277(5334), 1956-1962.

Taylor, B., K. Zellmer, F. Martinez, and A. Goodliffe (1996), Sea-floor spreading in the Lau back-arc basin, Earth Planet. Sci. Lett., 144, 35-40.

Tivey, M. (2010), Magnetic Analysis Code for Download, http://deeptow.whoi.edu/download.html.

Watanabe, M., K. Okino, and T. Kodera (2010), Rifting to spreading in the southern Lau Basin: Variations within the transition zone, Tectonophysics, 494, 226-234.

Weissel, J. K. (1977), Evolution of the Lau Basin by the growth of small plates, in Island Arcs, Deep Sea Trenches and Back-Arc Basins, Maurice Ewing Ser., vol. 1, edited by M. Talwani and W. C. Pitman III, 429-436, AGU, Washington, D. C.

Wessel, P., and W. H. F. Smith (1991), Free software helps map and display data, Eos Trans. AGU, 72(41), 441-446.

Wessel, P., and W. H. F. Smith (1998), New, improved version of Generic Mapping Tools released, Eos Trans. AGU, 79(47), 579.

Wessel, P., and L. Kroenke (2000), Ontong Java Plateau and late Neogene changes in Pacific plate motion, J. Geophys. Res, 105, 28255-28277.

Wessel, P., and L. Kroenke (2007), Reconciling late Neogene Pacific absolute and relative plate motion changes, Geochem. Geophys. Geosyst., 8(8), Q08001, doi: 10.1029/2007GC001636.

Wetzel, L. R., D. A. Wiens, and M. C. Kleinrock (1993), Evidence from earthquakes for bookshelf faulting at large non-transform ridge offsets, Nature, 362, 235-237.

Whelan, P. M., J. B. Gill, E. Kollman, R. A. Duncan, and R. E. Drake (1985), Radiometric dating of magmatic stages in Fiji, in Geology and offshore resources of Pacific island arcs—Tonga region, edited by D. W. Scholl and T. L. Vallier, 415-440, Circum Pacific Council for Energy and Mineral Resources, Houston, TX.

Wysoczanski, R. J., E. Todd, I. C. Wright, M. I. Leybourne, J. M. Hergt, C. Adam, and K. Mackay (2010), Backarc rifting, constructional volcanism and nascent disorganised spreading in the southern Havre Trough backarc rifts (SW Pacific), J. Volcanol. Geoth. Res., 190, 39-57.

Zellmer, K. E., and B. Taylor (2001), A three-plate kinematic model for Lau Basin opening, Geochem. Geophys. Geosyst., 2(5), 1020, doi: 10.1029/2000GC000106.